UILU-ENG 88-3604

Report No. 143

POST-WELD LASER-TREATMENT OF 18 Ni (250) MARAGING STEEL

by

Grzegorz Banas
Department of Civil Engineering
(Visiting Scholar from Politechnika Rzeszowska, Poland)

James Michael Rigsbee
Department of Materials Science and Engineering

Frederick V. Lawrence, Jr.
Department of Civil Engineering
Department of Materials Science and Engineering

A Report of the

MATERIALS ENGINEERING - MECHANICAL BEHAVIOR

College of Engineering, University of Illinois at Urbana-Champaign

July 1988

TABLE OF CONTENTS

POST-WELD LASER-TREATMENT OF 18 Ni (250) MARAGING STEEL

ABSTRACT

This investigation studied fatigue resistance of post-weld laser-treated 18 Ni (250) maraging steel. High powered laser-dressing of the weld toe was studied. An AVCO-Everett High-Power CO_2 Laser with helium shielding gas was used to perform this process.

Macro- and microstructural examinations were conducted to characterize the microstructure, hardness and fatigue crack initiation sites resulting from the as-welded and the post-weld treated specimens.

Fatigue strength predictions were made using the I-P model assuming validity of the K_{fmax} concept and predicted residual stress effects. The analytical predictions were compared with experimental data.

I. INTRODUCTION

1.1 Recent Trends

The fatigue resistance of a welded structure is almost always governed by that of its welds; consequently, much research has been devoted to the understanding and improvement of weld fatigue behavior. Post-weld treatments for fatigue life improvement have been developed; see Fig. 1. Some treatments give better results than others and complete recovery of the "lost" fatigue life can be obtained; e.g. shot peening most effectively increased the fatigue life followed closely by laser-dressing and lastly by GTA dressing for welded ASTM A514 structural grade steel [1], and grinding and shot peening of weldments increased the fatigue life up to that of the base metal for N18K9M5TPr maraging steel [2]. Ion implantation used with this steel affected the fatigue resistance very little [3].

Material properties in critical regions of weldments such as the HAZ can vary considerably depending on the heat input, joint details, plate thickness and weld process. However, the resulting differences in microstructure and hardness generally have only a minor effect on weld resistance because the severity of the notch and residual stress effects generally overshadow the metallurgical variables. Therefore, no method which improves weld fatigue resistance by improving material properties has been utilized. However, improvement of material properties accompanies most post-weld treatments shown in Fig. 1 [4].

Of the many factors, there are two which significantly affect the fatigue resistance of weldments: geometry and surface residual stresses.

1.1.1 Geometry

Fatigue cracks generally initiate and propagate from discontinuities in weldments. Many investigators have tried to predict when and where this will occur. Harrison [5], Gurney [6], Maddox [7], and Frank [8] assumed that all internal discontinuities were crack-like-defects or that there were preexisting cracks at external discontinuities after fabrication; therefore, the fatigue crack initiation life (N_I) was said to be negligibly short or nonexistent. Under this assumption, the total fatigue life (N_T) of welds was considered to be the fatigue crack propagation life (N_P) of welds which could be estimated using linear elastic fracture mechanics (LEFM) concept.

However, the work of Lawrence and Munse [9], and Lawrence and Burk [10] suggested that the fatigue life of butt welds with a crack-like-defects could not be explained solely by crack propagation and that the initiation life was found to comprise as much as half the total fatigue life. Also, studies by Lawrence [11], and Burk and Lawrence [12] on A36 butt welds showed that a significant portion of fatigue life was spent in initiation a 0.25 mm (0.01 in.) fatigue crack at the weld toe and that unrealistically small values of initial crack length would be required, especially in the long life region, to account for total fatigue life. In addition, Smith and Smith [13] measured fatigue cracks in the filled weld by the potential drop method and found that at a stress ratio of R = 0.17 initiation life occupied as much as 39% of the total fatigue life (1.5×10^6 cycles). Thus, it does not seem proper to consider all discontinuities to be crack-like-defects because the initiation life may be appreciable, and neglecting it may be excessively conservative. Moreover, it is doubtful that there is always a preexisting crack in a sound weld.

In the absence of weld defects, the major stress concentration in a specimen containing a transverse butt weld left in the as-welded condition occurs at the weld toe (Fig. 2). Having had advantageous weld toe shape (notch root radius (r) and flank angle (Θ)) the fatigue strength of weldment can reach that of the base metal [14] under conditions that $r = \infty$ and $\Theta = 0$. In order to obtain this kind of weldment, machining and grinding were used. Weld fatigue life improvement through changing the geometry of the weld toe is used more often because it is more economical [15]; e.g. grinding, GTA-dressing and recently laser-dressing. This treatment changes the notch root radius and the flank angle is that as for as-welded state.

1.1.2 Surface Residual Stresses

When a weld deposit cools, contraction of the hot weld metal is restrained by adjacent material, and this contraction causes tensile residual stresses in the weld metal and adjacent material upon cooling. Normally, the residual stresses in the toe of a weld will reach the magnitude of the yield point of the base metal.

It is currently accepted that residual stresses (whether introduced by the welding or introduced during subsequent treatment) may be treated as mechanical overstress and can thus be considered to be additive to the applied stresses [16, 17, 18, 19, 20].

The influence of residual stresses on the fatigue life of weldments has been reviewed and summarized by Curney [14], Munse [21], Pollard and Cover [22], Kelsey [23], and Reemsnyder [24]. Tensile residual stresses at the weld toe decrease the fatigue resistance of a weld. Stress relief (no residual stresses) improves weld fatigue resistance by reducing the tensile residual stresses. The compressive residual stresses improve the fatigue

resistance [20, 25, 26]. Burk [20] found that when A514 F butt welds were overloaded above 690 MPa before testing so as to induce compressive residual stress (-830 MPa assumed), their fatigue strength was twice that of as-welded welds. Lawrence and Ho [25] also found that overstressing GTA dressed A514 F butt welds before testing resulted in plain plate failure instead of weld toe failure. Also, Booth [26] studied shot-peened, non-load-carrying fillet welds and found that plain plate failure occurred. It seems possible, therefore, that compressive residual stresses may permit the recovery of the fatigue life lost through welding.

Of the techniques that produce compressive residual stresses, shot peening is mostly used because it brings about considerable improvement in fatigue resistance and it is economically attractive [15]. The exploding foil-flyer-plate technique and laser shock process (both techniques are called shock-loading) have been developed recently. Shock waves created while processing, cause plastic deformation of the treated zone and induce compressive residual stresses and consequent by increased tensile strength [27, 28, 29, 30]. The E.O. Paton Welding Institute has developed ultrasonic technique [31] and explosion treatment [32] that are competitive with other methods of improving the fatigue strength of welded joints, and there are as effective as work-hardening for butt joints made out of high strength steel.

1.2 Models for Weldment Fatigue Life Prediction

Empirical expressions for the fatigue strength of weldments subjected to either axial or bending loads have been suggested [33 - 41]. The propagation model has been developed by Maddox [33] and El Haddad [34] in which the total fatigue life (N_T) is predicted solely through estimates of

the fatigue crack propagation life (N_p). Lawrence et al., [35 - 41] have developed a hybrid, initiation-propagation (I-P) model in which the total life (N_T) is predicted by combining estimates of the fatigue crack initiation life (N_I) and the fatigue crack propagation life (N_p).

Weldments are generally subjected to both axial and bending loads; the latter often results from the straightening of fabrication induced distortions under load. Thus, the combined effects of axial and bending loads must be considered in estimating weldment fatigue strength. For fatigue lives greater than 10^5 cycles, the local stress-strain response to the applied remote stress amplitude (S_a) and the nominal mean stress (S_m) can be assumed to be elastic. Thus, the local mean stress (σ_m) and stress amplitude (σ_a) at the notch root can be expressed as [41]:

$$\sigma_m = \sigma_r + \left(K^A_{fmax}\, S^A_m + K^B_{fmax}\, S^B_m\right) \tag{1}$$

$$= \sigma_r + \frac{1+R}{1-R}\left(K^A_{fmax}\, S^A_a + K^B_{fmax}\, S^B_a\right) \quad \text{since } S_m = \left(\frac{1+R}{1-R}\right) S_a$$

where (σ_r) is the notch-root residual stress and (R) is the stress ratio. Also,

$$\sigma_a = \left(K^A_{fmax}\, S^A_a + K^B_{fmax}\, S^B_a\right) \tag{2}$$

From Basquin's relationship and Eqs. 1 and 2;

$$\sigma_a = \left[\sigma'_f - \sigma_r - \frac{1+R}{1-R}\left(K^A_{fmax} S^A_a + K^B_{fmax}\, S^B_a\right)\right]\left(2N_I\right)^b \tag{3}$$

Rearranging Eq. 3, the fatigue strength of weldment at long lives ($N_T > 10^5$ cycles) is:

$$S_a = \frac{\left(\sigma'_f - \sigma_r\right)\left(2N_I\right)^b}{K^{eff}_{fmax}\left[1 + \frac{1+R}{1-R}\left(2N_I\right)^b\right]} \tag{4}$$

$$K^{eff}_{fmax} = (1 - x)\, K^A_{fmax} + x\, K^B_{fmax} \tag{5}$$

$$x = S_a^B / S_a^T$$

$$S_a^T = S_a^A + S_a^B$$

A comparison of fatigue strength predictions made using Eq. 4 and experimental data for both as-welded and post-weld treated steel weldments is given in Fig. 3 [42].

1.3 Scope

This investigation focuses on increasing the fatigue resistance of welded 18 Ni (250) maraging steel through laser-dressing and overstressing. Fatigue data of the as-welded, laser-dressed, and prestressed condition were collected to compare the effects of these improving methods. Experimental fatigue strengths under a 2×10^6 cycle regime were compared with those of predicted fatigue strengths using Eq. 4.

II. EXPERIMENTAL PROGRAM AND RESULTS

Different post-weld treatments were used for the fatigue resistance improvement of weldments during this study. Fig. 4 shows the block diagram which includes, for a given weldment type, the heat treatment and the different combinations of laser-treatment and overstressing subsequently used.

The experimental program includes specifically:

- specimen preparation
- post-weld treatment
- fatigue tests
- microstructural observations.

2.1 Material

The 18 Ni (250) maraging steel was used in this study which had the composition and the monotonic, cyclic, and fatigue properties (after aging) given in Tables 1 and 2. The filler metal of similar composition was used during welding.

2.2 Specimen Fabrication

The 18 Ni (250) maraging steel was derived as a plate with the thickness of 4.15 mm which was saw-cut into smaller plates that included ten test-pieces. Bead-on-plate weldments were fabricated by depositing a weld bead on both sides of the plate using a semi-automatic GMA welding apparatus the processing parameters of which are given in Table 3. Test pieces were saw-cut into strips which were subsequently subjected to different post-weld treatments.

Bead on Plate As-Welded (AW). The strips were machined to dimensions shown in Fig. 5 and heat-treated.

Bead on Plate Overstressed (AW-OS). The strips were machined to dimensions shown in Fig. 5, heat-treated and overstressed.

Laser Dressed Aged (LDA). The strips were laser-dressed, machined to dimensions shown in Fig. 5 and heat-treated.

Laser Dressed Aged-Overstressed (LDA-OS). The strips were laser-dressed, machined to dimensions shown in Fig. 5, heat-treated and overstressed.

Laser Dressed (LD). The strips were machined to dimensions shown in Fig. 5, heat-treated and laser-dressed.

Laser Dressed Overstressed (LD-OS). The strips were machined to dimensions shown in Fig. 5, heat-treated, laser-dressed and overstressed.

2.3 Post-Weld Treatments

The heat treatment, laser-dressing and overstress were used as the post-weld treatments.

2.3.1 Heat Treatment

Aging at 480°C for 5 hours is the standard heat treatment for the 18 Ni (250) maraging steel after welding. This process produces intermetallic precipitates which gives the steel mechanical properties listed in Table 2.

2.3.2 Laser-Dressing

An AVCO-Everett High Power CO_2 Laser with helium shielding gas was used to perform the laser-dressing of the weldments. This laser produces a beam of 10.2 μm continuous radiation at powers up to 10 kW. A fixed laser

beam defocused with a f18 focusing mirror to an annular circle of 5 mm diameter was used to obtain a proper irradiated area and to avoid any possible damage caused by refocusing of the beam through back reflection. The beam impingement angle was 10° from the plate normal. The plates were moved horizontally beneath the beam at a constant speed. Helium shielding gas was directed along the weld toe at 6.8 m^3/h through an oblong (25.4 x 6 mm) nozzle positioned to give maximum coverage to the molten and cooling regions during the treatment: see Fig. 6. The surfaces of the weld toes were coated with ultra-black paint to maximize the absorption of energy.

The process parameters (Table 4) and experimental geometries (Fig. 6 and 7) to obtain desirable toe configuration were established after series of preliminary tests for the particular geometry and material used in this investigation.

2.3.4 Overstress

A 20 kip MTS machine was used to overstress the weldments. The tensile load up to the yield point (1,700 MPa) of the base metal was applied in order to induce the compressive residual stresses. The overstressing was applied just before the fatigue test of each specimen; see Fig. 4 -- AW-OS and LD-OS.

2.4 Fatigue Testing and Results

The fatigue tests were carried on in the conventional manner utilizing the 20 kip MTS machine with self-aligning grips using a sine wave form, load control, a zero-to-max. stress cycle (R = 0) and frequency of 10 Hz. There were considerable bending stresses due to the fact that the specimens were not perfectly straight.

2.4.1 Bending Stresses

The bending stresses were estimated using two micro-measurements strain gauges (6.4 mm, 120 Ω) which were attached to both sides of each specimen using M-bond 200 adhesive (cyanoacryle). A proper distance (one-third of the plate thickness) from the weld toe (or new toe) to the strain gauges [36, 44] was maintained so as the monitored strains would be independent of the weld toe stress concentration and would approximate the nominal surface strain. The bending strains were measured under small axial loads (0-to-4 kN) prior to cycling and calculated considering the magnitude of strains measured on both sides of the specimen. The results of these calculations and fatigue test results are shown in Tables 5 through 9.

2.4.2 Results

The results of fatigue tests for the cases indicated in Fig. 4 (AW, AW-OS, LDA, LDA-OS, and LD) are shown in Figures 8 trough 13. Only few data points were available for AW-OS and LDA-OS. The slopes of the S-N curves were calculated using Eq. 18.

The summary of the fatigue test results is shown in Fig. 13. Laser-dressing and overstress played significant role in the fatigue resistance improvement of weldments. The overstressing of laser-dressed weldments (LDA-OS) increased the fatigue strength the most, followed closely by overstressing of as-welded (AW-OS) specimens. Laser-dressing of the aged weldments (LD) is less effective than laser-dressing of the unaged (LDA) specimens. The main reason for this was a presence of the undercuts in the LD weldments produced during laser-dressing while the laser beam was entering and leaving the laser-treated zone. The machining would remove

those undercuts. But due to the high hardness of the LD weldments (52 HRC) after aging, the machining had to be done before aging and laser-dressing. The LDA weldments did not have any undercuts because they were machined and aged after laser-dressing (p. 2.2).

2.5 Microstructural Observations

Laser-treatment altered the geometry, microstructure, mechanical properties and location of the fatigue crack initiation sites. Regions of interest were examined with optical (OM), scanning electron (SEM), and transmission electron (TEM) microscopes. Microhardness traverses were performed using a Leitz microhardness tester.

The macrographs and micrographs of cross-section for as-welded (AW) and laser-dressed specimens (LDA and LD) are shown in Figures 14 trough 16. The composition of the filler metal was the same as the base metal. Consequently, both the weld and base metal had the same basic microstructure. Both consist of a low-carbon martensite matrix which hardens through the precipitation of intermetallic compounds on aging [45]. The laser-dressed HAZ includes several regions which differ one from another depending on the amount of reverted austenite (white pools: see Fig. 14), which is soft and stable. The reverted austenite does not harden when the joint is aged. Consequently, the regions with reverted austenite remained softer than the rest of the HAZ zone structure [45]. The amount of reverted austenite depends on the welding or laser-dressing heat input. Since the amount of reverted austenite increases with heat input, one would expect the strength to decrease as the heat input increases. This trend is shown in a plot of ultimate strength versus heat input (Fig. 17).

The OM examinations of laser-dressed weldments (LD, LDA) a surface layer which looked different from the WM and HAZ, despite aging was performed either before or after laser-dressing: see Figures 15 and 16. The SEM examinations showed a great deal of reverted austenite in laser-treated zones (Figures. 15b and 16c). To prove existence of reverted austenite in the laser-treated zone, a TEM study was undertaken.

Fig. 18 shows a series of TEM bright-field and dark-field micrographs and a corresponding selected area electron diffraction pattern for a laser-treated and aged (LDA) zone. In this region, the reverted austenite is present in a predominantly low-carbon body-centered cubic "lath" martensite matrix as seen in the bright-field image shown by Fig. 18a. This particular micrograph does not clearly show the existence of austenite. The dark-field images (Figs. 18 b and c) show a great deal of reverted austenite visible as small white needles, possible due to local enrichment in nickel which favors austenite formation [46]. The small needles (approx. 85 nm long by 5 nm diameter) interspersed within the martensite matrix and in some cases much larger austenite patches are present at prior austenite grain boundaries: see region "A", Fig. 18c. Electron diffraction indicates the existence of Ni_3Ti and Ni_3Mo precipitates within the martensite [47], [48]. Identification of the various phases was done with selected area electron diffraction: see Figs. 18d and e.

Fig. 19a shows a bright-field image corresponding to the aged laser-treated (LD) zone. Reverted austenite is again visible as small needles interspersed within the martensite matrix. Identification of the phases was done with selected electron diffraction: see Figs. 19 b and c. No precipitates have been identified, presumably due to the effect of heat

input while laser dressing, which may be regarded as solutionizing heat treatment after which low-carbon martensite is formed upon cooling [46].

Figures 20a and 21a show bright-field images of weld metal and base metal, respectively. The microstructure is similar to those described above; however, no reverted austenite has been found in the base metal. Ni_3Ti and Ni_3Mo precipitates are visible in both the weld and the base metal regions. Identification of the phases was done with selected electron diffraction: see Figures 20 b, c, and 21 b, c.

Knoop hardness traverses for as-welded (AW) and laser-dressed (LD and LDA) specimens are plotted in Figures 22 - 24. Following ref. [45] the HAZ has been divided into three separate zones; nearest to the weld is a zone (A) that was heated into the fully austenitic region by the heat of welding and transformed to martensite on cooling, next to this is zone (B) that was heated into the two-phase austenite + ferrite field, and a zone (C) that experienced temperatures from approximately 500 °C to just above ambient. The new HAZ and molten metal zone (MM) have been created as a result of laser-dressing process (Figures 23 and 24).

The hardness in as-welded (AW) specimen does not vary significantly in the zones studied; however, a slight decrease in hardness was noticed in zone (C) as a result of reverted austenite that occurs due to welding process [45]. There were some soft regions in the base metal which might be attributed to improper hot rolling while manufacturing. Laser-dressing process significantly changes the distribution of Knoop hardness. The MM zone is much softer due to existence of reverted austenite and lack of precipitates (Figures 23 and 24). The hardness declines when laser-dressing is being performed after aging (LD) in both MM and the new HAZ (Fig. 24). This is the effect of heat input during laser-treatment. Besides, zone (C)

is much softer for that case (annealing effect) than it is for the case when laser-dressing was performed before aging: compare Figures 23 with 24.

Generally, a significantly soft surface layer is created by laser-dressing of welded 18 Ni maraging steel despite the post-weld aging was performed either before or after laser-treatment. The presence of stable reverted austenite that blocks precipitation of Ni_3Ti and Ni_3Ti in this layer is the main reason for softening of the laser-treated zone. Besides, heat input due to welding and laser-dressing process causes solutionizing heat treatment after which low-carbon martensite is formed upon cooling without any precipitates within it.

2.6 Fatigue Crack Initiation Sites

The as-welded toe profiles in Fig. 25a and clearly show the variation of toe radius along its length. The variability of the toe radius apparent in this figure supports the basic idea of the K_{fmax} concept that all radii are present in a given region. Dressing treatments significantly altered the curvature of the original toe and produced a new toe at the intersection between the dressing bead and the plate surface with associated new HAZ: see Figures 23a, 24a, 25b and 25c. Properly executed laser-dressing with high degree of control over the location and motion of the molten pool, could produce a very straight new fusion line with very smooth, nearly imperceptible undercut along the length of the new toe [4]. In fact, this new toe was generally undercut to some degree. This fact plays an important role in the fatigue fracture of the dressed welds (Figures 25 b and c).

Each of the as-welded specimens failed at the weld toe. Fatigue cracks started from the surface (Fig. 26a), usually at the place where the smallest radius occurred ($r \geq 0.1$ mm).

Most laser-dressed failures initiated at the new weld toe, despite the fact that aging was performed either after or before laser-treatment. Figures 26b and 27 show fracture surfaces with indications of the crack initiation sites which were located at the surface near the new weld toe (MM zone: see Figures 23a and 24a). This area was relatively softer due to reverted austenite formed after laser-treatment. In some cases specimens failed either at the HAZ or even in the base metal.

III. FATIGUE STRENGTH PREDICTIONS

The post-weld treatments used in this study significantly altered one or more of the major factors which influence the total fatigue life: geometry, residual stresses, and material properties. The I-P model developed by Lawrence et al. was used to predict the fatigue strength of the as-welded (AW) and laser-dressed (LDA and LD) weldments.

3.1 Application of the I-P Model to Laser-Dressed Weldments

Early experiments showed that dressing process altered geometry of the weld toe and produced a new toe at which there was a slight undercut. Moreover, the hardness of laser-dressed zone was lower than that of the weld metal and HAZ.

3.1.1 Stress Concentration Factor (K_t)

To determine (K_t) of a new toe, a model was developed which considered the geometry of the new toe with undercut to be a big notch (weld toe) with a small surface notch (undercut): see Fig. 28. The stress concentration factor (K_t^g) for a weld toe was calculated by Mattos and Lawrence [49] using FEM:

$$K_t^g = 1 + \alpha\left(t/r_g\right)^{1/2} \tag{6}$$

where (t) is the plate thickness and (r_g) is the radius of big geometry. The stress concentration factor for a general surface notch is:

$$K_t^n = 1 + 2\left(d/r_n\right)^{1/2} \tag{7}$$

where (d) is notch depth (undercut depth) and r_n is notch root radius. If a weld toe has a surface notch, the stress concentration factor (K_t^s) at the surface notch root can be estimated by superposing the two value of (K_t): see Fig. 28b:

$$K_t^s = K_t^g \times K_t^n \tag{8}$$

Substituting Eqs. 6 and 7 into Eq. 8:

$$K_t^s = \left[1 + \alpha(t/r_g)^{1/2}\right]\left[1 + 2(d/r_n)^{1/2}\right] \tag{9}$$

Here, (t) and (α) are known and (r_g) can be measured.

Therefore, (K_t^s) can be expressed:

$$K_t^s = C\left[1 + 2(d/r_n)^{1/2}\right] = C + 2C\left[d/r_n\right]^{1/2} \tag{10}$$

where $C(\geq 1)$ is a constant representing the calculations of the first term with known values in Eq. 10. Thus, the fatigue notch factor (K_f^s) can be expressed:

$$K_f^s = 1 + \frac{K_t^s - 1}{1 + \underline{a}/r_n} = 1 + \frac{C - 1 + 2C\left[d/r_n\right]^{1/2}}{1 + \underline{a}/r_n} \tag{11}$$

For (K_{fmax}^s) condition:

$$\frac{dK_f^s}{dr_n} = 0 \tag{12}$$

As a result, (K_{fmax}^s) occurs when $r_n = r_M$:

$$r_M = \left[\frac{\underline{a}(C - 1) + \left[(C - 1)^2\underline{a}^2 + 4\underline{a}C^2d\right]^{1/2}}{2Cd^{1/2}}\right]^2 \tag{13}$$

Since notch depth (d) can be measured, (r_M) can be evaluated numerically. Therefore, (K_{fmax}^s) can be estimated by substituting the value of (r_M) into Eq.11.

The depth of the undercut at possible crack initiation sites was measured using a profilometer for laser-dressed weldments. The profiles and depths are shown in Fig. 29. The root radius of undercut showed sufficient variation to support the use of the (K_{fmax}) condition in each case. For the case of a surface notch on a flat surface, (C) is unity. Then, from Eq. 13, (K_{fmax}) occurs when $r_M = \underline{a}$, which is the same result as Lawrence et al. [35] found in a simple, as-welded geometry.

3.1.2 Residual Stresses (σ_r)

The maximum compressive residual stresses of high strength steels can be obtained as a function of either tensile strength or hardness [4]:

$$\sigma_r = -(0.21\ S_u + 550) = -(0.9\ BHN + 550) \qquad (14)$$

However, as a rule of thumb, (σ_r) for laser-dressed 18 Ni (250) maraging steel can be assumed to be negative value of 50 - 60% of the tensile strength before laser-treatment:

$$\sigma_r = -(0.5 - 0.6)\ S_u \qquad (15)$$

This assumption was confirmed by estimation of the residual stresses of laser-dressed 18 Ni (250) maraging steel bead-on-plate weldments. The longitudinal (axial) residual stresses were measured at both the toes and at the top of the welds using an X-ray residual stress apparatus. The irradiated spot was 2.5 mm diameter with an X-ray surface penetration; penetration depth was less than 5 μm. The results are given in Table 10.

This assumption, however, does not apply to the as-welded specimens; residual stresses in the weld metal were about 20% smaller than those predicted. According to ref. [45], residual compressive stresses are set up

while welding 18 Ni (250) maraging steel. It is due to the austenite to martensite transformation at comparatively low temperatures, that causes increase in volume and sets up opposing compressive stresses that are large enough to neutralize and overcome the tensile stresses, that were before transformation due to the heat input while welding. Therefore the measured values given in Table 10. should be considered to be the results of heat input and austenite to martensite transformation while welding and post-weld treatment; laser-dressing.

3.1.3 Determination of Fatigue Properties

Hardness traverses of the laser-dressed zone showed that its hardness varied significantly and was about 25% lower than that of the base metal (Figures 23 and 24). Since the crack initiation takes place very near the surface, the material at the depth (a_I) will respond to the local stresses and determine the crack initiation life of the structure. Therefore, the material properties determined from hardness measured at the depth of crack initiation (a_I) were used in the prediction of the fatigue strength.

The ultimate strength was estimated from hardness measurements:

$$S_u^{LDZ} = S_u^{BM} \frac{DPH_{LDZ}}{DPH_{BM}} \tag{16}$$

where (S_u^{LDZ}) is the ultimate strength of laser-dressed zone, (S_u^{BM}) is the ultimate strength of the base metal, (DPH_{LDZ}) is the hardness of laser-dressed zone, and (DPH_{BM}) is the hardness of the base metal.

The fatigue strength coefficient (σ_f') and fatigue strength exponent (b) were calculated using equations [50]:

$$\sigma'_f = 3.3\ DPH_{LDZ} + 370 \tag{17}$$

$$b = -\frac{1}{6}\log\left[2\left(1 + \frac{191}{S_u^{LDZ}}\right)\right] \tag{18}$$

Young's modulus (E) was assumed to be unaffected by the post-weld treatments.

3.3 Comparison of Predictions with Experiments

Experimental results for as-welded (AW) and laser-dressed (LDA) specimens were compared with those of predicted using Eq. 4. There is a good agreement within the high cycle fatigue between experimental results and predictions for laser-dressed (LDA) weldments. The only difference is in the slope which is: $b = -0.0282$ for the experimental results, and $b = -0.0597$ for the prediction. This means that the notch radius of the laser-dressed area significantly affected the initiation portion of the fatigue life within the tested weldments.

Predictions for the as-welded (AW) case underestimated the fatigue strength having almost the same slope (b) as it was for experimental results. This difference came out probably from the fact that I-P model used for these predictions was developed for weldments made out of thicker plates. In this case the thickness of the welded strips was 4.15 mm. That fact was presumably the main reason for the difference shown in Fig. 30.

IV. CONCLUSIONS

1. Laser-dressing was found to be an effective method of improving the weld fatigue strength of 18 Ni (250) maraging steel. More advantageous geometry and compressive residual stresses were the factors that mainly affected the fatigue strength.
2. Reverted austenite was produced by the laser-dressing treatment and was found to be metastable and relatively softer than the HAZ.
3. It appears that the I-P model as presented herein can predict the weld fatigue strength for the laser treatment studied in this investigation.

ACKNOWLEDGEMENTS

The authors thank Prof. C. M. WAYMAN for supplying the material; J. L. KOCH for assistance in the laser-dressing of weldments, and B. REYNOLDS for welding of specimens. Many colleagues deserve special credit for the encouragement and ideas given to the authors during this study.

Doctors Z. KHAN and P. KURATH are thanked for their invaluable assistance in the laboratory. The authors also acknowledge Dr. S. K. PARK for his suggestions related to the fatigue strength analysis, and Dr. C. P. JU is thanked for his assistance in the analysis of TEM micrographs.

Grateful acknowledgements are made to D. BLUNIER of Caterpillar Technical Center, Peoria, Illinois, for his kind assistance in measuring residual stresses, and to Dr. C. BEGG for chemical analysis of 18 Ni (250) maraging steel.

Fracture Control Program and Materials Processing Consortium of the College of Engineering at the University of Illinois are acknowledged for the support given to the authors.

REFERENCES

1. Murzyn, P.J.,: "An Experimental Study of the Means for Improving Weldment Fatigue Resistance", M. Th. University of Illinois, Metallurgical Engineering, 1981.

2. Report No. ZTM/U-855/79,: "Badania wplywu nagniatania dynamicznego na jakosc zlaczy spawanych ze stali N18K9M5TPr", Politechnika Rzeszowska, 1979.

3. Report No. ZTM/U-977/85,: "Badania wplywu umocnienia na okres inicjacji pekniec zmeczeniowych w zlaczach spawanych ze stali N18K9M5TPr", Politechnika Rzeszowska, 1985.

4. Chang, S.-T., Lawrence, F.V. Jr.,: "Improvement of weld fatigue resistance", A Report on Fracture Control Program, No. 46, January 1983.

5. Harrison, J.D.,: "An Analysis on the Fatigue Behavior of Cruciform Joints", Brit. Weld. Inst., Report No.E/21/12/68, 1968.

6. Gurney, T.R.,: "A Revised Analysis of the Influence of Toe Defects on the Fatigue Strength of Transverse Non-Load-Carrying Fillet Welds", Weld. Res. Intl., Vol. 9, No. 3 p. 43, 1979.

7. Maddox, S.J.,: "Fracture Mechanics Applied to Fatigue in Welded Structure", Brit. Weld. Inst. Report No. E/36/70, 1970.

8. Frank, K.H.,: "The Fatigue Strength of Fillet Welded Connections", Ph.D. Thesis, Leighi University, 1971.

9. Lawrence, F.V. Jr., and Munse, W.H.,: "Fatigue Crack Propagation in Butt Welds Containing Joint Penetration Defects", Weld. J. Vol. 52, p. 221s, 1973.

10. Burk, J.D., and Lawrence, F.V. Jr.,: "Effects of Lack of Penetration and Lack of Fusion on the Fatigue Properties of 5083 Aluminum Alloy Welds", Weld. Res. Council Bull. Vol. 4, No. 4, 1979.

11. Lawrence, F.V. Jr.,: "Estimation of Fatigue Crack Propagation Life in Butt Welds", Weld. J. Vol. 52, pp. 212s-220s, 1973.

12. Burk, J.D., and Lawrence F.V. Jr.,: "Influence of Bending Stresses on Fatigue Crack Propagation Life in Butt Joint Welds", Weld. J. Vol. 56, p. 43s, 1977.

13. Smith, I.F.C., and Smith, R.A.,: "Measurement of Fatigue Crack in Welded joints", Int. J. Fatigue, vol. 4, No. 1, p. 42, 1981.

14. Gurney T.R.,: "Fatigue of Welded Structures", Sec. Edition, Cambridge University Press, Cambridge, 1979.

15. Harrison J.D., et al.,: "A Summary of Techniques for Improving the Fatigue Strength of Welded Structures and an Estimate of their Cost", Fatigue Performance of Welded High Strength Steels, A Compendium of Reports from a Sponsored Research Program, The Welding Institute, Albinghton Hall, Albinghton-Cambridge CB16AL, England, 1974.

16. Morrow, JoDean, Ross, A.S., and Sinclair, G.M.,: "Relaxation of Residual Stresses due to Fatigue Loading", TAM Report No. 568, University of Illinois, Urbana, Ill., 1959.

17. Mottos, R.J.,: "Estimation Fatigue Initiation Life of Weld", Ph.D. Thesis, University of Illinois, Urbana, Ill., 1973.

18. Lomacky, O., Ellingwood, B., and Figgord. L.N.,: "Analysis of Low Cycle Fatigue Performance of Welded Structural Joints", Trans. 3rd Int. Conf. on Structural Mechanics in Reactor Technology, Vol. 5, Part L, L6/6, 1976.

19. Smith, K.N., El Haddad, M., and Martin, J.F.,: "Fatigue Life and Crack Propagation Analyses of Welded Components Containing Residual Stresses", J. Mat. and Eval., Vol. 5, No. 4, p. 327, 1977.

20. Burk, J.D.,: "Effect of Residual Stresses on Weld Fatigue Life", Ph.D. Thesis, University of Illinois, Urbana, Ill., 1978.

21. Munse, W.H.,: "Fatigue of Welded Steel Structure", Weld. Res. Council, New York, 1964.

22. Pollard, B., and Cover, R.J.,: "Fatigue of Steel Weldments", Weld. J., Vol. 51, No. 11, p. 544s, 1972.

23. Kelsey, R.A.,: "Fatigue and Fracture Characteristics of Al Mg Butt Welds", Alcoa Lab., Report No. 57-77-18, 1977.

24. Reemsnyder H.S.,: "Evaluating the Effect of Residual Stress on Notch Fatigue Resistance", Symposium on Residual Stress, ASTM, Phoenix, 1981.

25. Ho, N,-J., and Lawrence F.V. Jr.,: Unpublished results, Dept. of Metallurgical Engineering, University of Illinois, Urbana, Ill., 1979.

26. Booth, G.S.,: "The Fatigue Life of Ground or Peened Fillet Weld Steel Joints - the Effect of Mean Stress", Metal Constr., Vol. 13, No. 2, P. 38-42, 1981.

27. Ford, S.C., et al.,: "Investigation of Laser Shock Processing -- Executive Summary", Technical Report AFWAL-TR-80-3001, Vol. 1, August, 1980.

28. Clauer, A.H., et al.,: "Laser Shock Hardening of Weld Zones in Aluminum Alloys", Metallurgical Transactions A, Vol. 8A, p. 1871 - 1876, December, 1977.

29. Larouche, S., et al.,: "Strengthening Effects of Deformation Twins and Dislocations Introduced by Short Duration Shock Pulses in Cu-8.7Ge", Metallurgical Transactions A, Vol. 12A, p. 1777 - 1785, October, 1981.

30. Meyers, Marc A.,: "Discussion of 'Residual Strength of Shock Loaded RMI 38644'", Metallurgical Transactions A, Vol. 8A, p. 1641 - 1644, October, 1977.

31. Mikheev, P.P., et al.,: "Effectiveness of ultrasonic treatment in improving the fatigue strength of welded joints", Automatic Welding, p. 37 - 40, March, 1984.

32. Petushkov, V.G., and Kudinov, V.M.: "The Explosion Treatment of Welded Joints", Automatic Welding, Vol. 38, No. 7, p. 3 -8, July, 1985.

33. Maddox, S.J.,: "Assessing the Significance of Flaws in Welds Subject to Fatigue", Welding Journal, p. 401s - 409s, 1974.

34. El Haddad, M.H., et al.,: "Fatigue Life Predictions of Welded Components Based on Fracture Mechanics", Journal of Testing and Evaluation, JTEVA, Vol. 8, No. 6, p. 301 - 307. 1980.

35. Lawrence, F.V., Jr., et al.,: "Estimating the Fatigue Crack Initiation Life of Welds", ASTM STP 648, p. 134 - 158, 1978.

36. Lawrence, F.V., Jr., et al.,: "Predicting the Fatigue Resistance of Welds", Amm, Rev. Mater. Sci., p. 401
425, 1981.

37. Tobe, Y., and Lawrence, F.V., Jr.,: "The Effect of Inadequate Joint Penetration on the Fatigue Resistance of High-Strength Structural Steel Welds", Welding Journal, Vol. 56, No. 9, p. 269s - 266s, 1975.

38. McMahon, J., and Lawrence, F.V., Jr.,: "Fatigue Crack Initiation and Early Growth in Tensile-Shear Spot Weldments", University of Illinois at Urbana-Champaign, Fracture Control Program, Report 131 UILU-ENG 86-3608, 1986.

39. Lawrence, F.V., Jr., et al.,: "A Fatigue Design Method for Weldments Based on Crack Initiation", International Conference on Fatigue of Welded Constructions, Paper No. 47, The Welding Institute, Abington Hall, Abington, Cambridge CB1 6AL, 1987.

40. Landgraf, R.W.,: "Effect of Mean Stress on the Fatigue Behavior of a hard steel", M.S. Thesis, University of Illinois at Urbana-Champaign, 1966.

41. Yung, J.-Y., Lawrence, F.V., Jr.,: "Analytical and Graphical Aids for the Fatigue Design of Weldments", Fatigue Fract. Engng Mater. Struct., 8 (3) p. 223 - 241, 1985.

42. Radziminski, J.B., at al.,: "Fatigue Data Bank and Data Analysis Investigation", Structural Research Series No. 405, Civil Engineering Studies, University of Illinois at Urbana-Champaign, June, 1973.

43. Kado, S., et al.,: "Fatigue Strength Improvement of Welded Joints by Plasma Arc Dressing", IIW/IIS-Doc.-XIII-774-75, Japan, 1975.

44. Burk, J.D.,: "Prediction of the Fatigue Crack Propagation Lives of Butt Weldments", Master's Thesis, Dept. of Metallurgy, University of Illinois at Urbana-Champaign, 1974.

45. Lang, F.H., Kenyon, N.,: "Welding of Maraging Steels", Welding Research Council, Bulletin No. 159, February, 1971.

46. Floreen, S.,: "Maraging Steels", Metals Handbook, Ninth Edition, Vol. 1, Properties and Selection: Iron and Steels, ASM.

47. Floreen, S.,: "The physical metallurgy of maraging steels", Metallurgical Reviews, Vol. 13, 1968.

48. Thomas, G., et al.,: "Precipitation in Fe-Ni-Co Alloys", Transactions of the ASM, Vol. 62, 1969.

49. Mattos, R.J., and Lawrence, F.V., Jr.,: "Estimation of the Fatigue Crack Initiation Life in Welds Using Low Cycle Fatigue Concepts", FCP Rep. No. 19, University of Illinois at Urbana-Champaign, 1975.

50. McMahon, J., Lawrence, F.V., Jr.,: "Predicting Fatigue Properties Through Hardness Measurements", FCP Rep. No. 105, University of Illinois at Urbana-Champaign, 1984.

Table 1
Chemical composition of Ni 18 (250) maraging steel. [a, b]

C%	Mn%	P%	S%	Si%	Ni%	Cr%	Mo%	Cu%	Ti%	Co%	Al%
0.02	0.01	0.008	0.007	0.08	18.29	0.03	5.40	0.04	0.34	7.31	0.01

[a], Chemical composition analysis was done by CHICAGO SPECTRO SERVICE LABORATORY, Inc.
[b], Iron -- balance.

Table 2
Mechanical properties of 18 Ni (250) maraging steel.

Monotonic Properties		
Elastic Modulus, GPa (ksi)	E	186 (26,867)
Hardness, HRC		50 - 52
Yield Strength (0.2%), MPa (ksi)	S_y	1,700 (247)
Ultimate Tensile Strength, MPa (ksi)	S_u	1,800 (260)
Reduction in Area	%RA	55
True Fracture Strength, MPA (ksi)	σ_f	2,146 (310)
True Fracture Ductility	ε_f	0.80
Strength Coefficient, MPa (ksi)	K	2,160 (312)
Strain Hardening Exponent	n	0.03
Cyclic Properties		
Fatigue Ductility Coefficient	ε_f'	0.80
Fatigue Ductility Exponent	c	-0.61
Fatigue Strength Coefficient, MPa (ksi)	σ_f'	2,232 (322)
Fatigue Strength Exponent	b	-0.063
Cyclic Strength Coefficient, MPa (ksi)	K'	2,282 (329)
Cyclic Strain Hardening Exponent	n'	0.10
Cyclic Yield Strength, MPa (ksi)	S_y'	1,245 (181)
Transition Fatigue Life, Reversals	$2N_t$	330
Propagation Properties		
Fracture Toughness, MPa$\sqrt{m}$ (R = 0)	K_c	85

Table 3
GTA welding parameters.

Plate Thickness, mm	4.15
Electrode Diameter, mm	2.3
Current, A	150
Voltage, V	24
Travel Speed, mm/s	1.7
Heat Input, kJ/mm	2.1
Shielding Gas	Argon
Gas Flow Rate, m^3/h	0.51
Gas Cup Size, mm	12.7

Table 4
Laser-dressing parameters.

Beam Impingement	80°
Shielding Gas	Helium
Shielding Gas Pressure, MPa	0.414
Shielding Gas Flow Rate, m^3/h	6.8
Shielding Gas Impingement Angle	8°
Beam Power, kW	4
Heat Input, kJ/mm	0.59
Focussing Mirror	f18
Distance to Focus from Surface, mm	50
Travel Speed, mm/s	6.8
Surface Coating	Ultra-black Paint

Table 5

Fatigue test results for as-welded (AW) specimens (R = 0).

Maximum Stress (MPa)	Bending Stress (MPa)	Fatigue Life (Cycles)	Failure Site	Comments
350	31	51,100	weld toe	
350	35	33,400	weld toe	
350	25	48,700	weld toe	
400	-	80,200	weld toe	
450	-	60,400	weld toe	
500	-	30,300	weld toe	

Table 6

Fatigue test results for as-welded and overstressed (AW-OS) specimens (R = 0).

Maximum Stress (MPa)	Bending Stress (MPa)	Fatigue Life (Cycles)	Failure Site	Comments
350	11	4,000,000	-	no failure
450	10	2,000,000	-	no failure
643	15	814,000	weld toe	
643	7	65,100	weld toe	
643	29	89,000	weld toe	

Table 7

Fatigue test results for laser-dressed and aged (LDA) specimens (R = 0).

Maximum Stress (MPa)	Bending Stress (MPa)	Fatigue Life (Cycles)	Failure Site	Comments
350	29	4,000,000	-	no failure
350	38	176,000	weld toe	
350	6	5,000,000	-	no failure
450	6	254,300	weld toe	
450	13	2,000,000	-	no failure
450	10	144,000	weld toe	
450	6	2,000,000	-	no failure
450	34	93,300	weld toe	
450	6	179,800	weld toe	
450	29	2,000,000	-	no failure
500	35	178,500	weld toe	
500	66	55,300	weld toe	
500	5	2,000,000	-	no failure
500	75	85,200	weld toe	
500	6	2,000,000	-	no failure
550	12	96,600	base metal	
550	29	72,600	base metal	
550	8	519,100	base metal	
600	5	1,103,000	weld toe	
600	20	86,800	weld toe	
643	30	44,300	weld toe	
643	15	61,000	weld toe	

Table 8

Fatigue test results for laser-dressed aged and overstressed (LDA-OS) specimens (R = 0).

Maximum Stress (MPa)	Bending Stress (MPa)	Fatigue Life (Cycles)	Failure Site	Comments
643	3	2,000,000	-	no failure
750	7	133,200	weld toe	
643	38	433,100	weld toe	

Table 9

Fatigue test results for laser-dressed (LD) specimens (R = 0).

Maximum Stress (MPa)	Bending Stress (MPa)	Fatigue Life (Cycles)	Failure Site	Comments
350	-	2,000,000	-	no failure
350	-	49,800	weld toe	
350	-	78,900	weld toe	
350	-	197,400	weld toe	
350	-	149,100	weld toe	
350	-	281,300	weld toe	
350	-	385,200	weld toe	

Table 10

Results of residual stress measurements.

Description	Location	Predicted Value using Eq. 15 (MPa)	Measured Value (MPa)
As-welded (AW)	Weld Metal (Center)	-(900 ÷ 1,080)	-756
	Toe	-(900 ÷ 1,080)	-333
Laser-dressed (LDA)	Weld Metal (Center)	-(900 ÷ 1,080)	-787
	Toe	-(900 ÷ 1,080)	-.1122

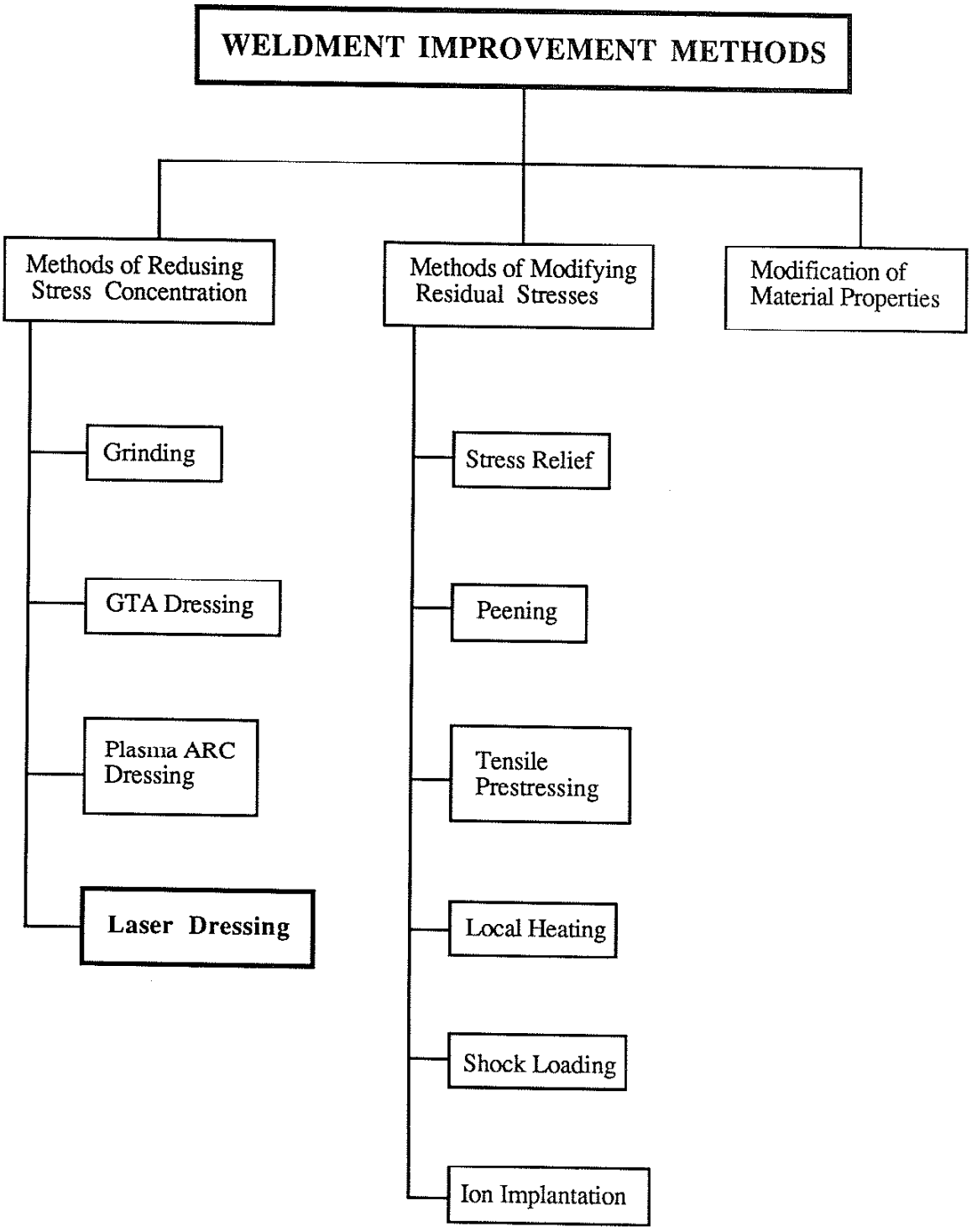

Fig. 1 Weldment improvement methods.

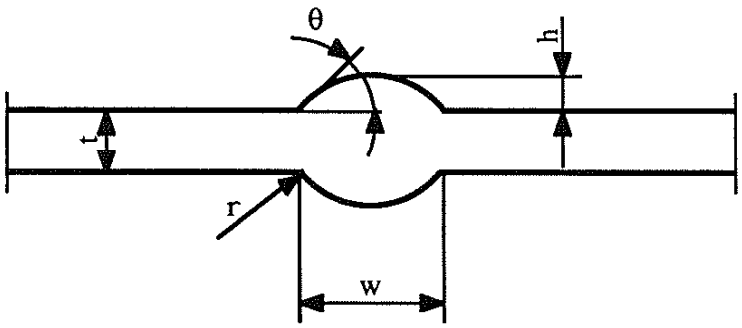

Fig. 2 Geometry of butt weld.

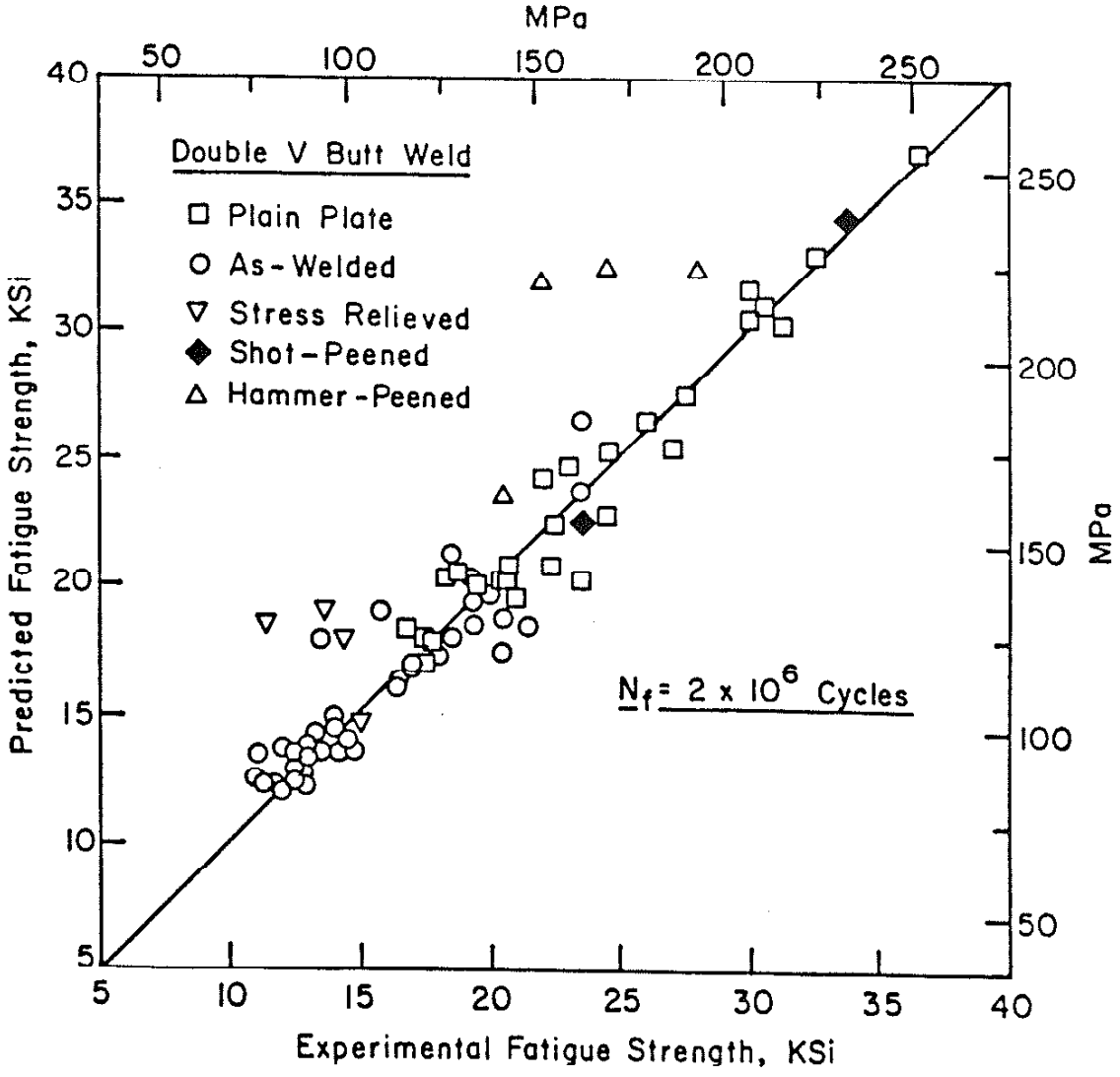

Fig. 3 Comparison of weldment fatigue strength predicted using Eg. 4 with experimental data principally from the UIUC Weldment Fatigue Data Bank [42].

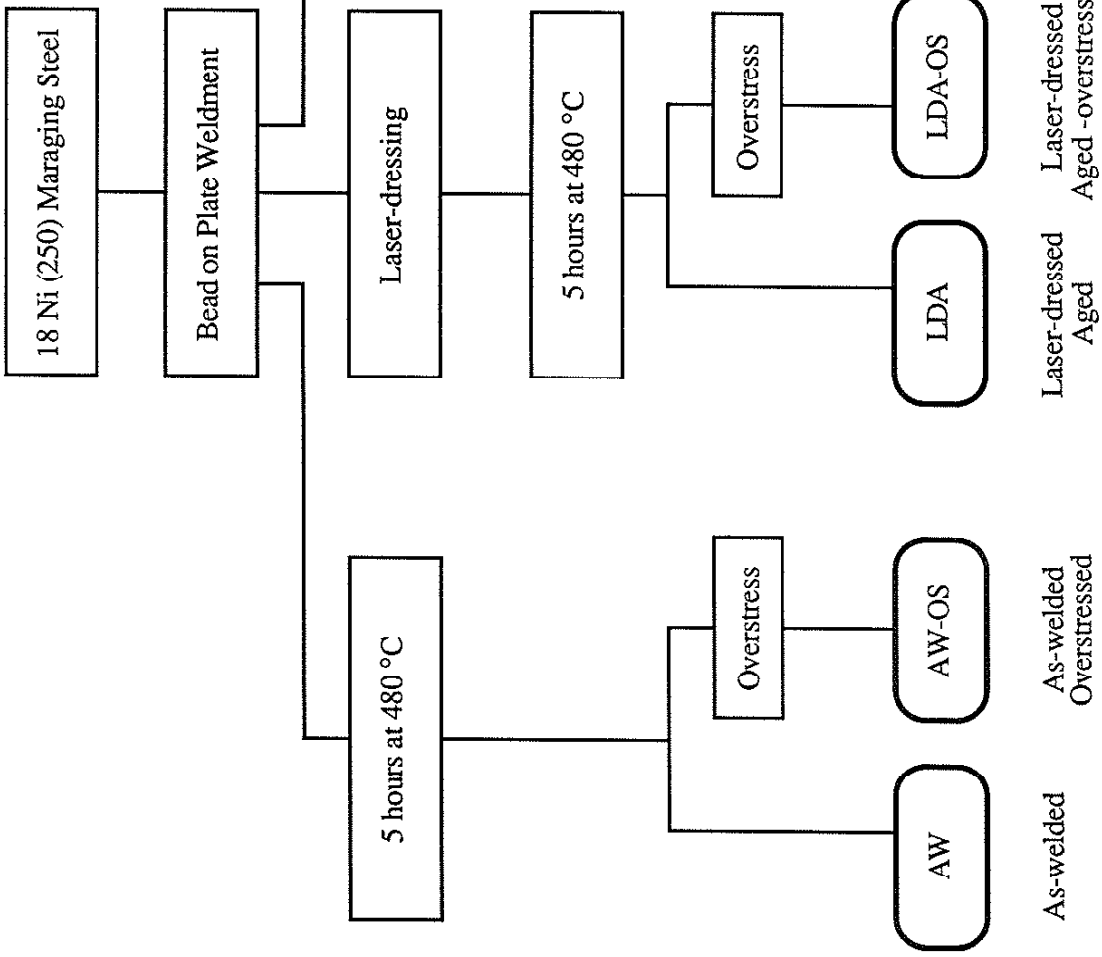

Fig. 4 Block diagram of the study.

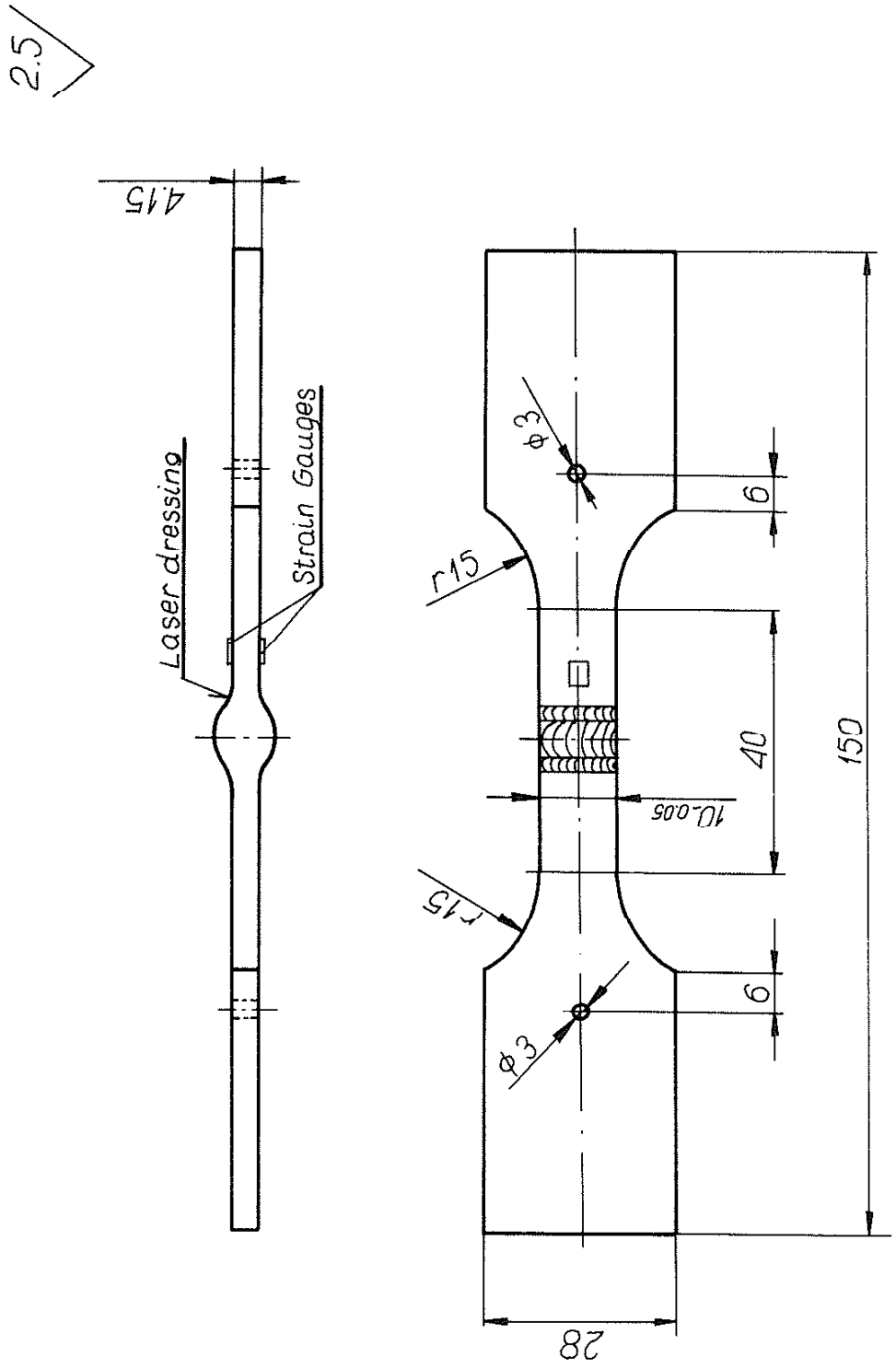

Fig. 5 Fatigue test piece of laser-dressed bead on plate.

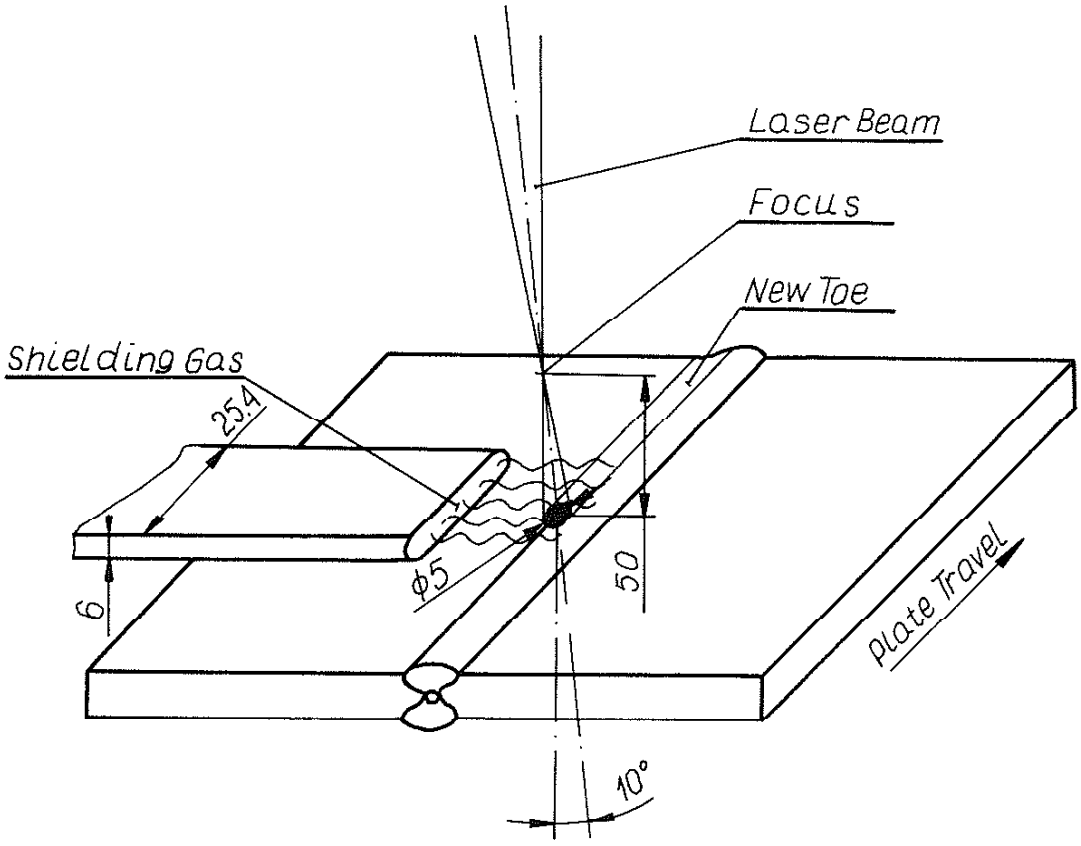

Fig. 6 Laser dressing set-up used in this study.

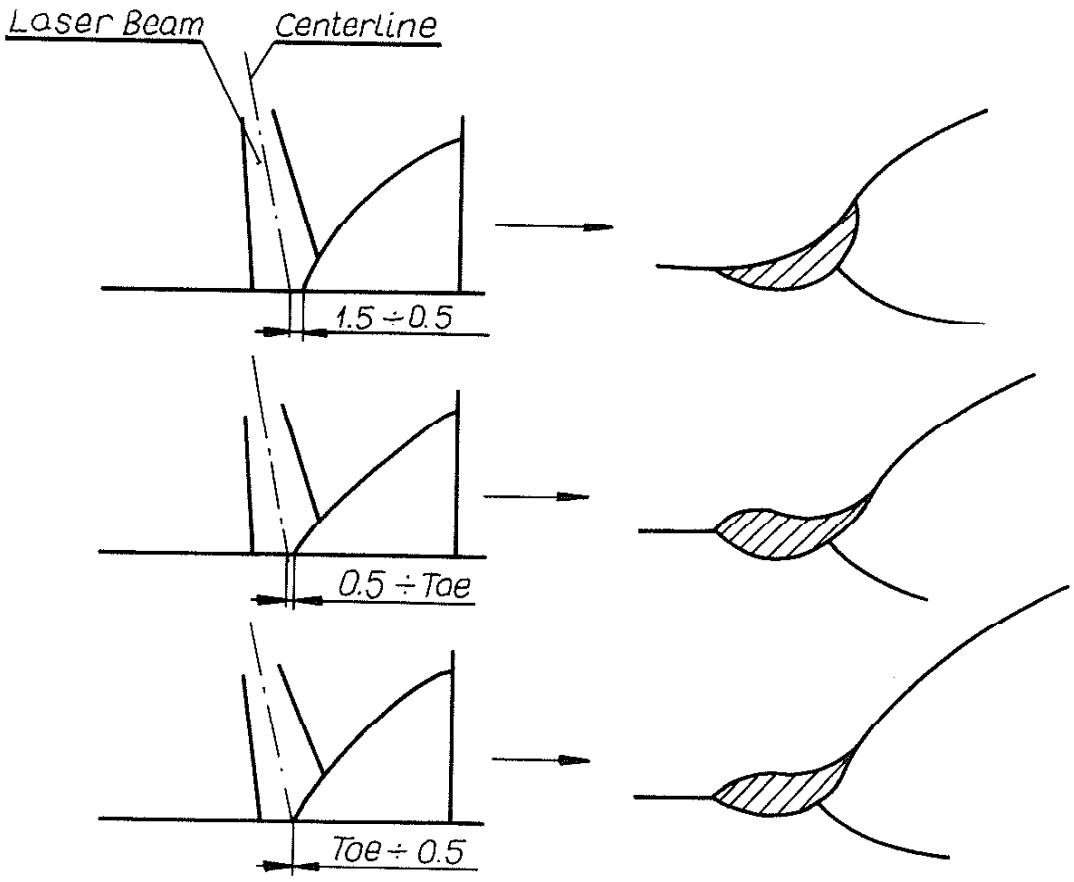

Fig. 7 Position of laser beam and resultant profiles after Kado et al. [43].

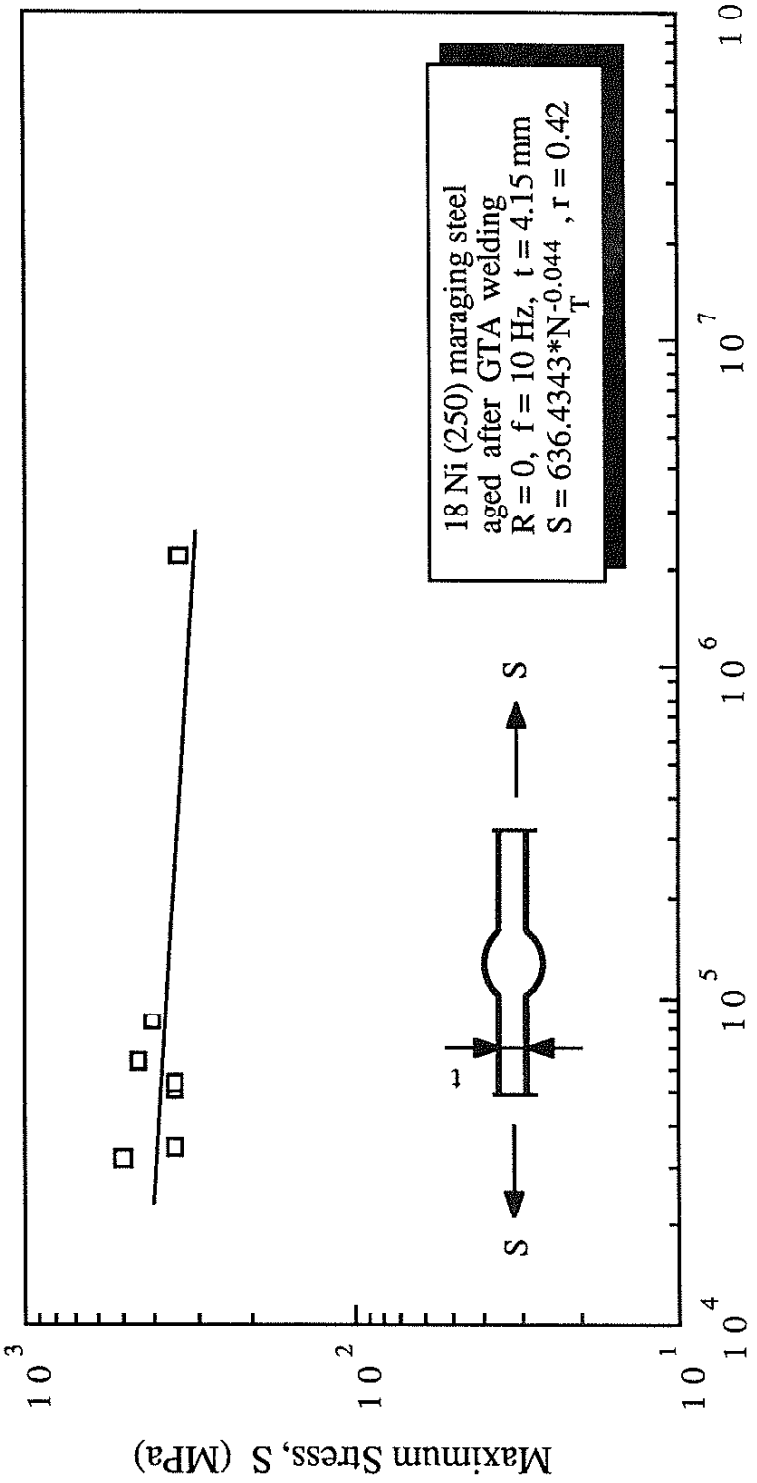

Fig. 8 Fatigue test results for AW weldments.

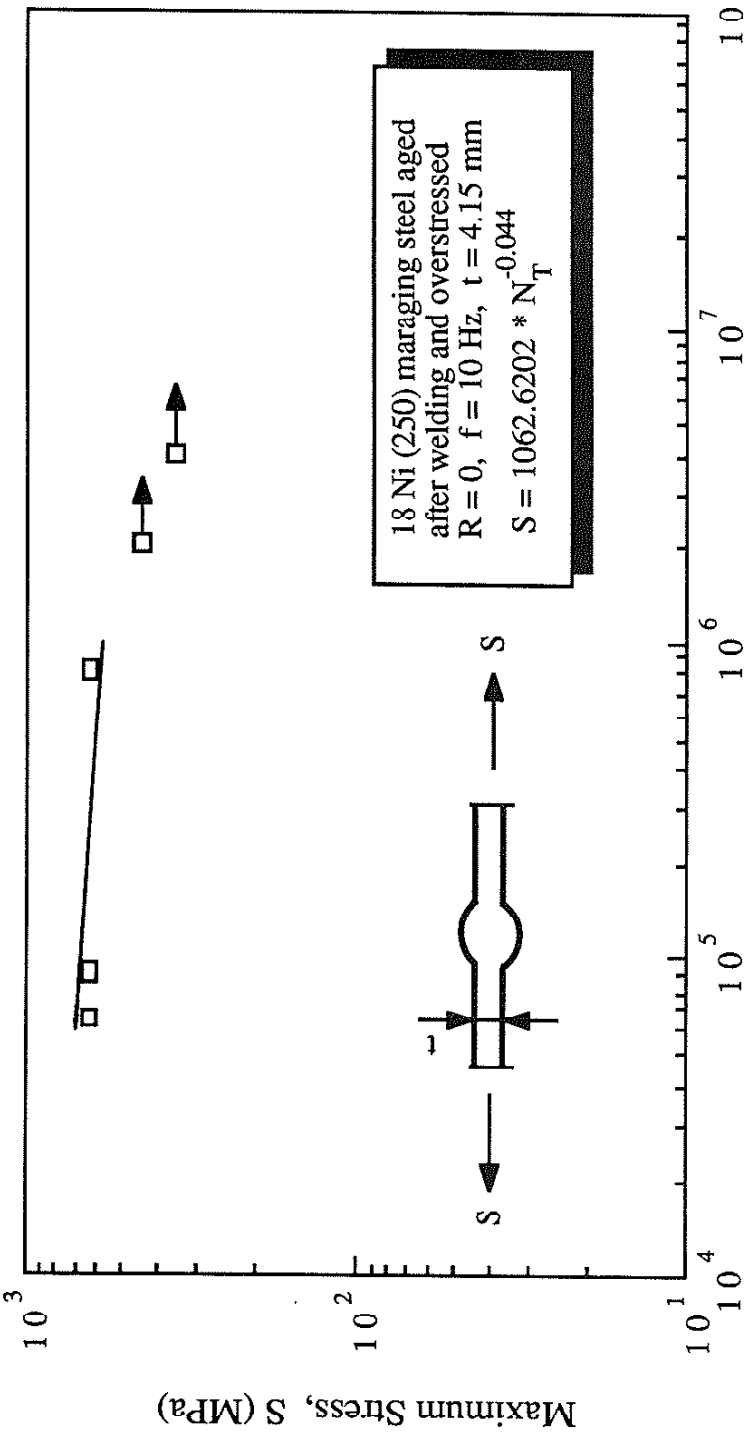

Fig. 9 Fatigue test results for AW-OS weldments.

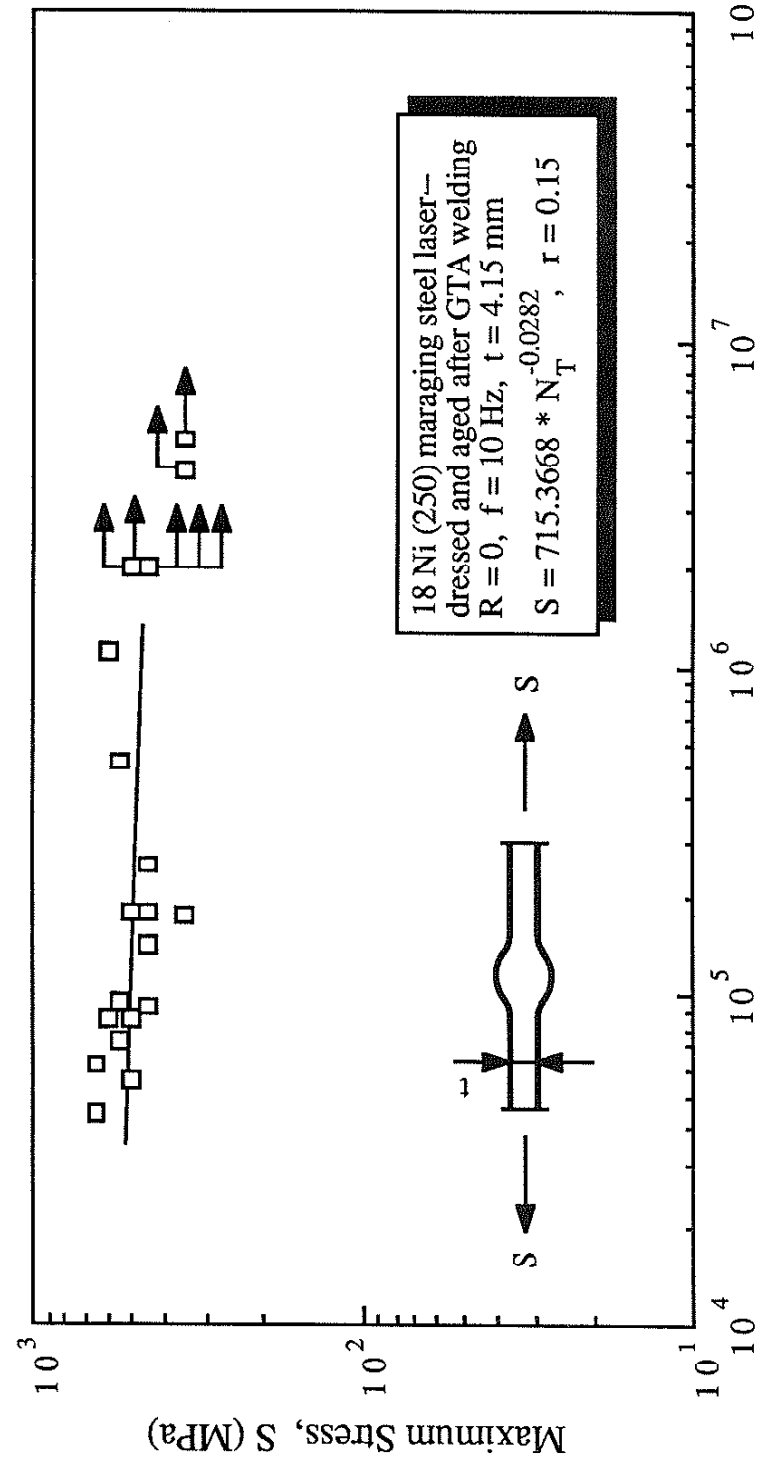

Fig. 10 Fatigue test results for LDA weldments.

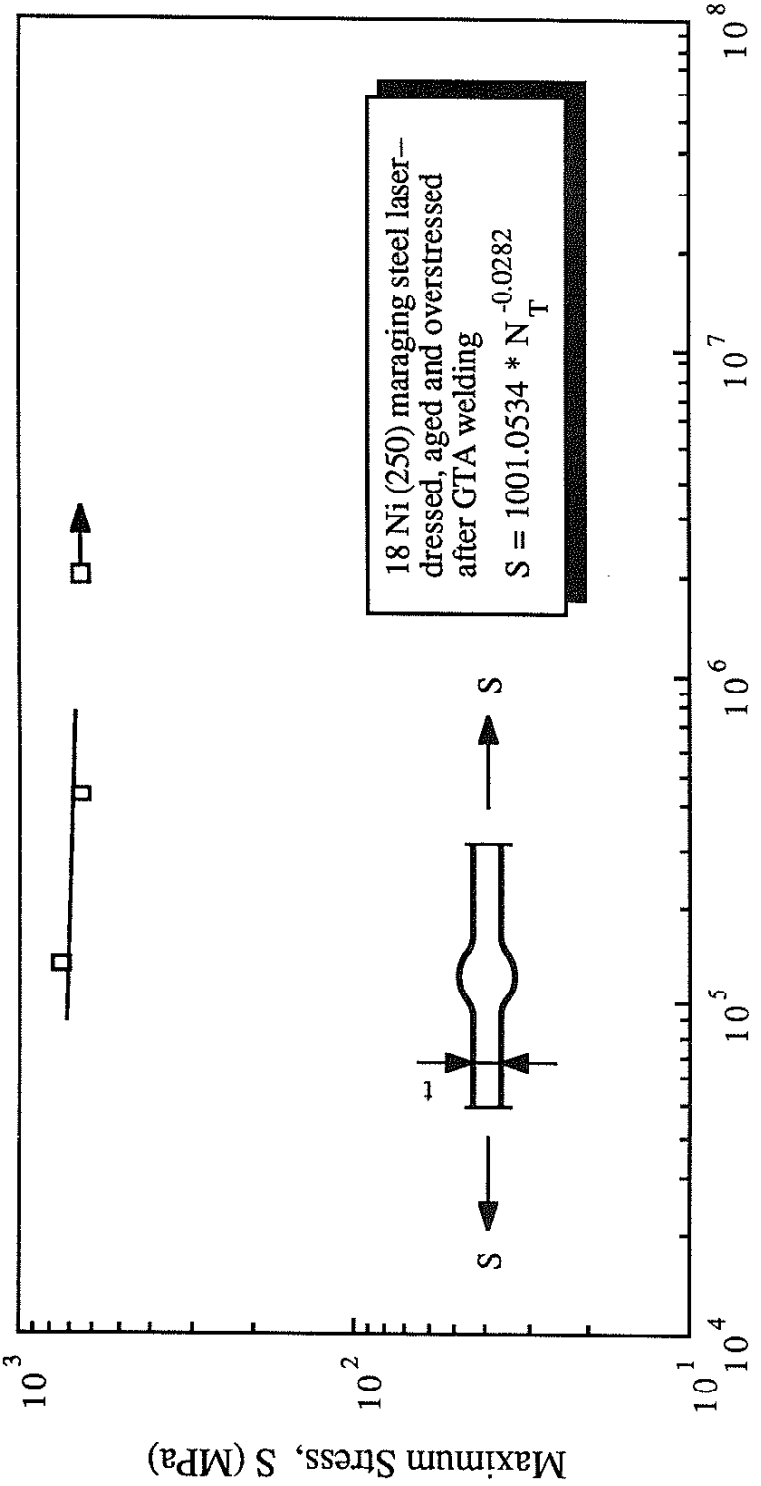

Fig. 11 Fatigue test results for LDA-OS weldments.

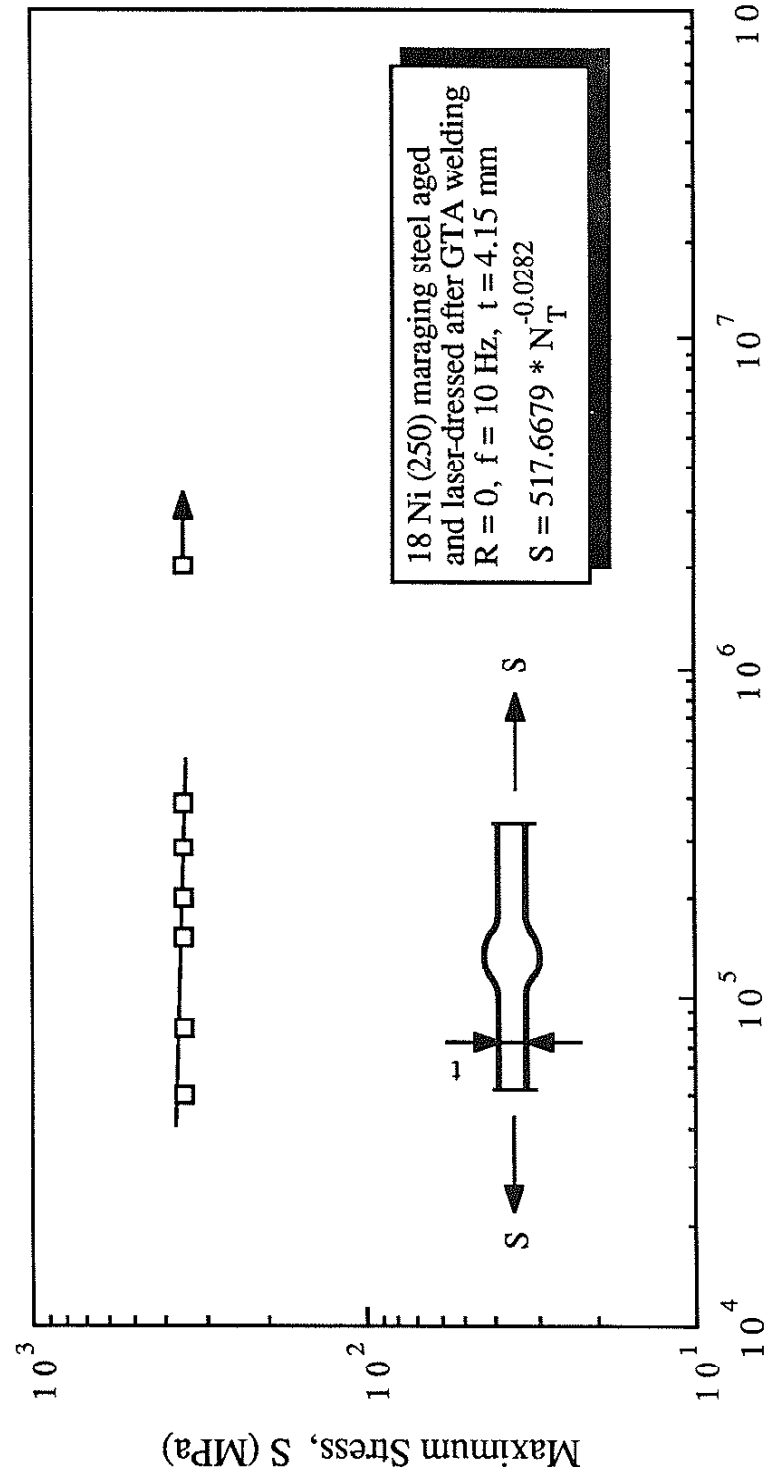

Fig. 12 Fatigue test results for LD weldments.

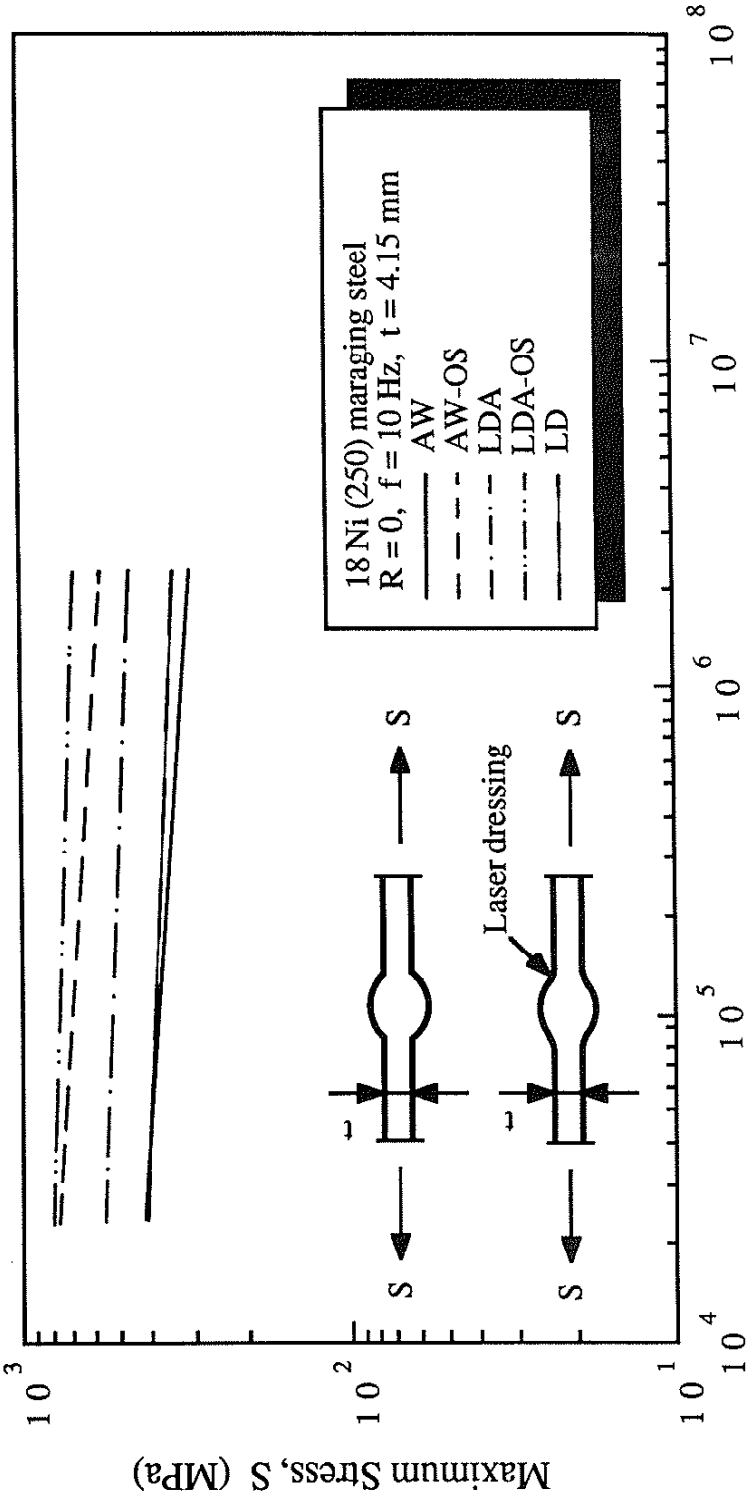

Fig. 13 Fatigue test results for as-welded and post-weld treated specimens.

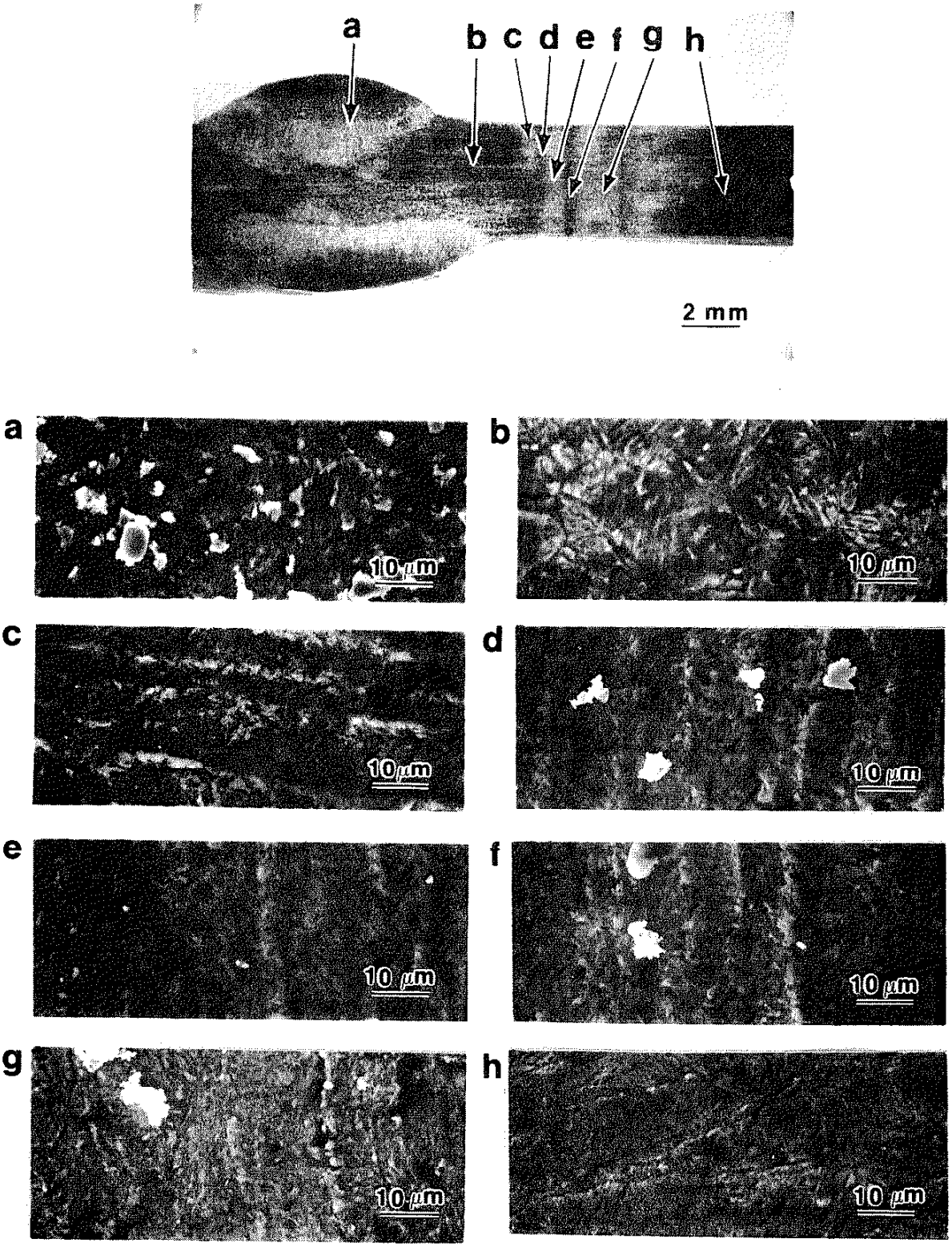

Fig. 14 Macrograph and micrograph of cross-section for as-welded (AW) 18 Ni (250) maraging steel. *Aging was performed after welding*: a) One-pass weld metal, b), c), d), e), f), g) Heat affected zone, h) Base metal.

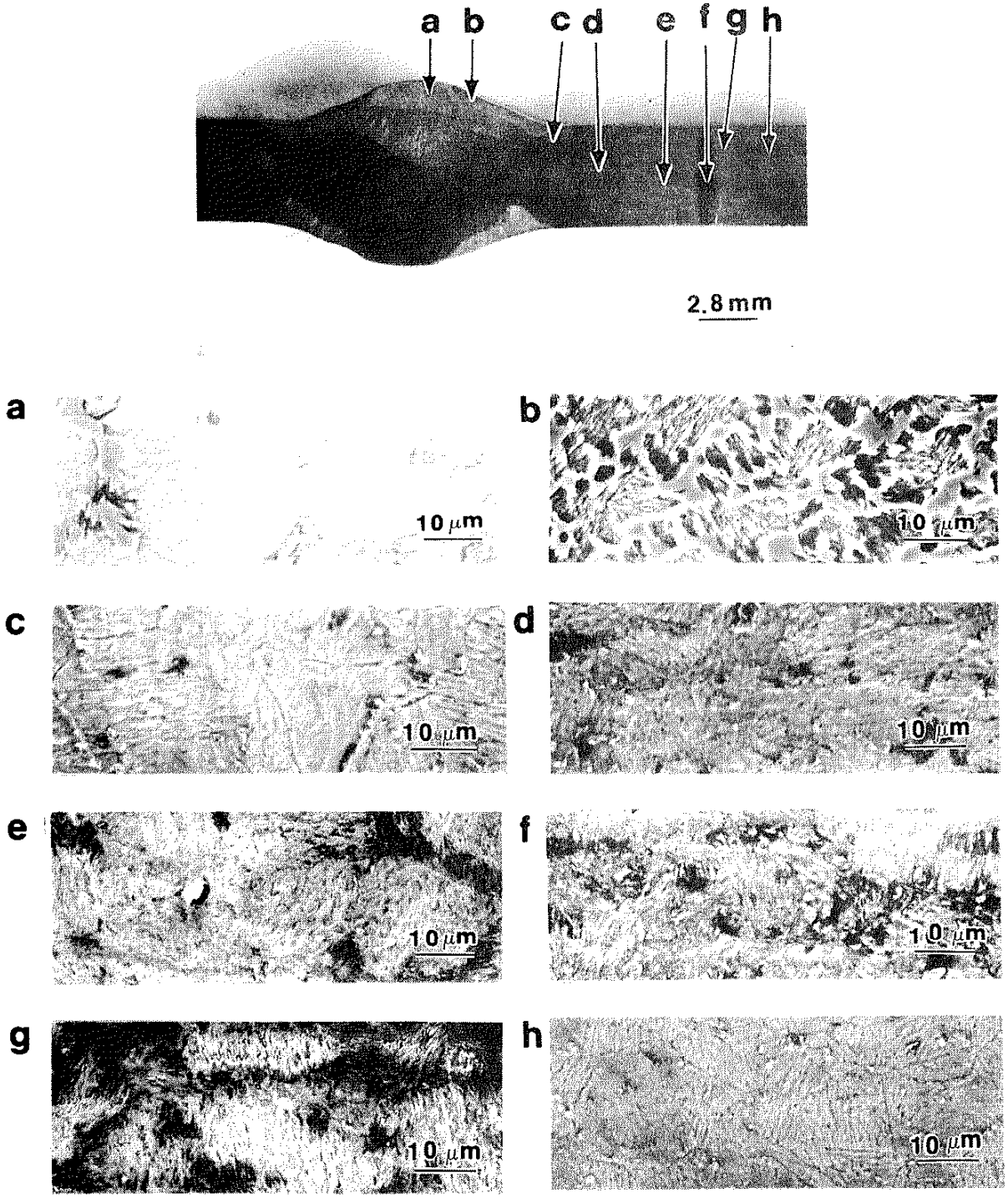

Fig. 15 Macrograph and micrographs of cross-section for welded and laser-dressed (LDA) 18 Ni (250) maraging steel. *Aging was performed after laser-dressing*: a) One-pass weld metal, b) Laser- treated area, c) New heat affected zone, d), e), f), g) Heat affected zone, h) Base metal.

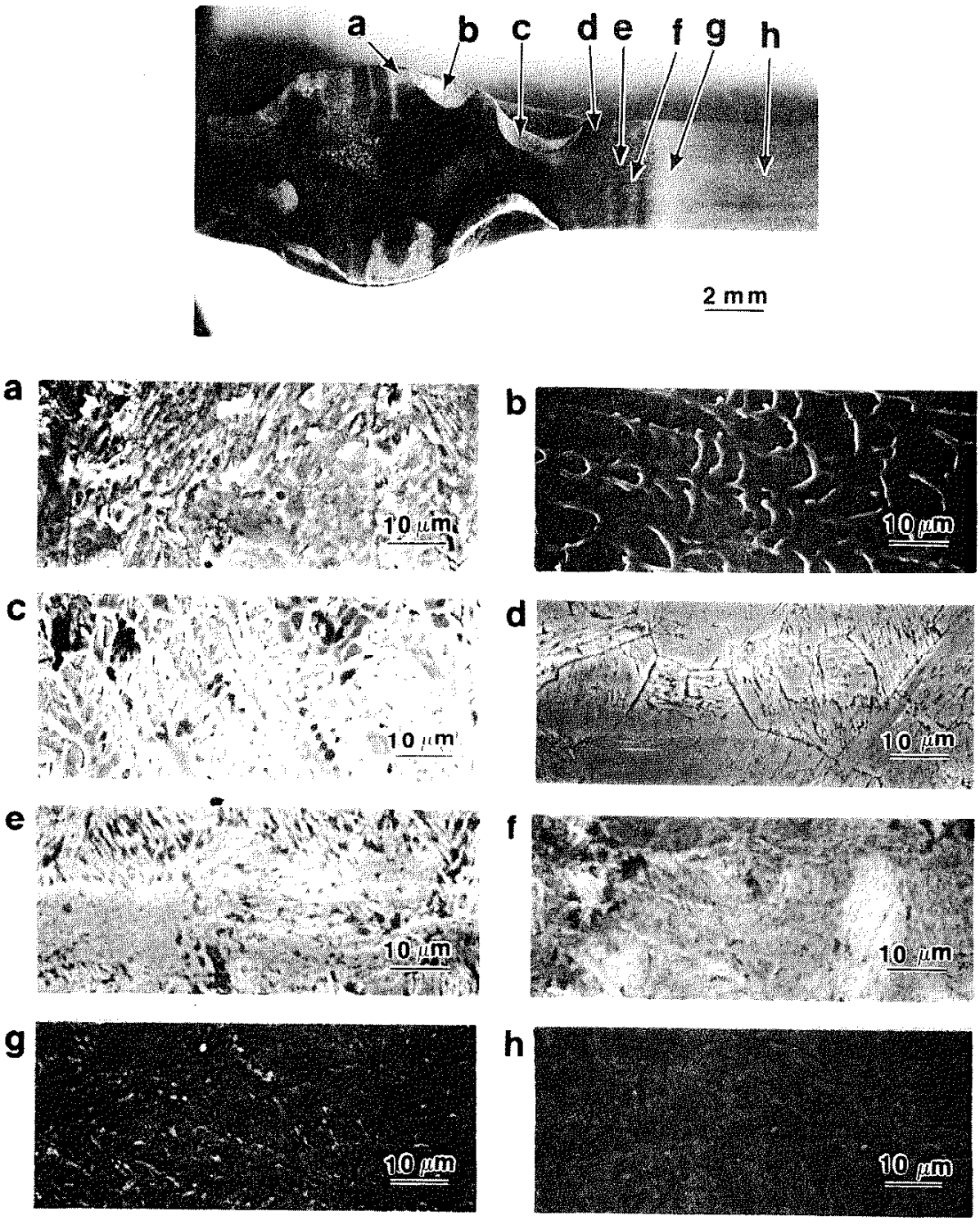

Fig. 16 Macrograph and micrographs of cross-section for welded and laser-dressed (LD) 18 Ni (250) maraging steel. *Aging was performed before laser-dressing*: a) One-pass weld metal, b) Two-pass weld metal, c) Laser-treated area, d) New heat affected zone, e), f), g) Heat affected zone, h) Base metal.

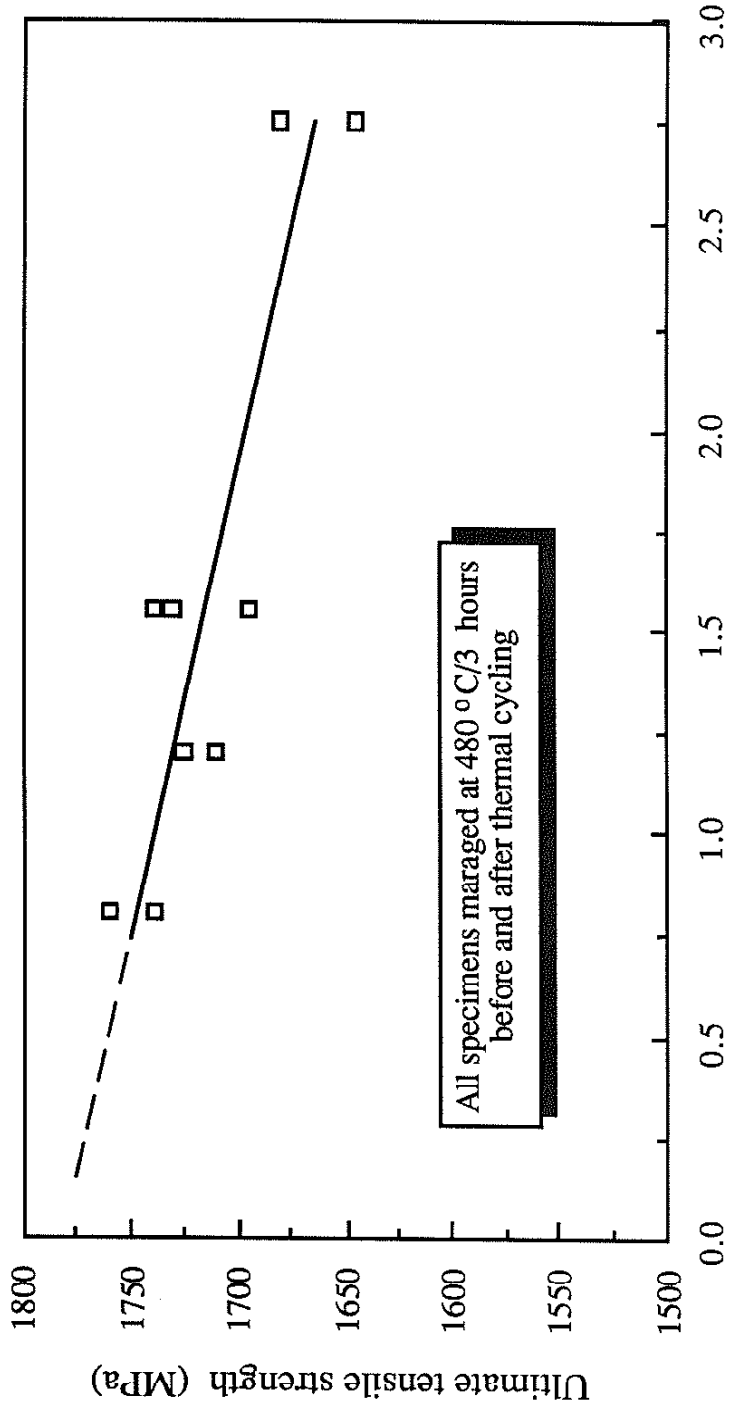

Fig. 17 Strength of specimens cycled to 650 °C peak temperature at varying energy input values [45].

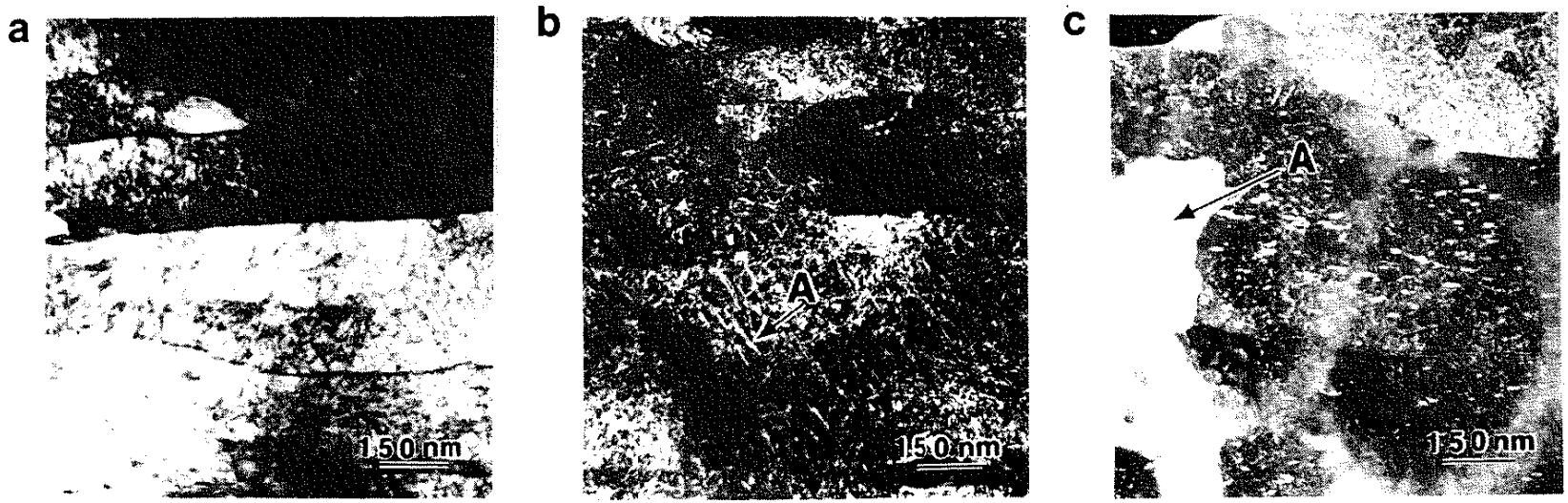

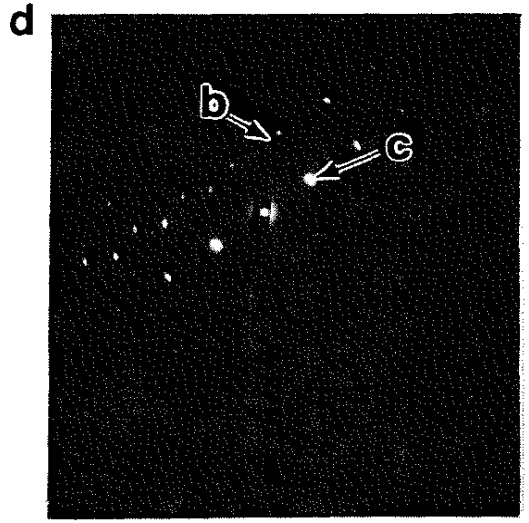

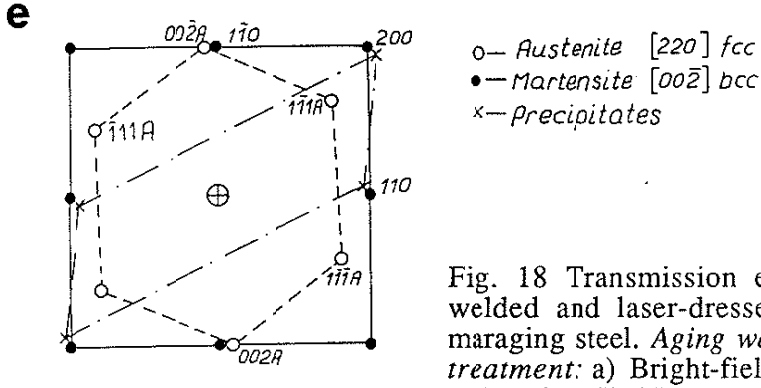

Fig. 18 Transmission electron micrographs of welded and laser-dressed (LDA) 18 Ni (250) maraging steel. *Aging was performed after laser-treatment:* a) Bright-field image showing a law-carbon bcc "lath" martensite matrix, b) Dark-field image of spot 110 bcc, shows reverted austenite as white needles (indice A), c) Dark-field image of spot 111 fcc, shows a great deal of reverted austenite (region A), d) Diffraction pattern, e) Sketch showing principal indexing.

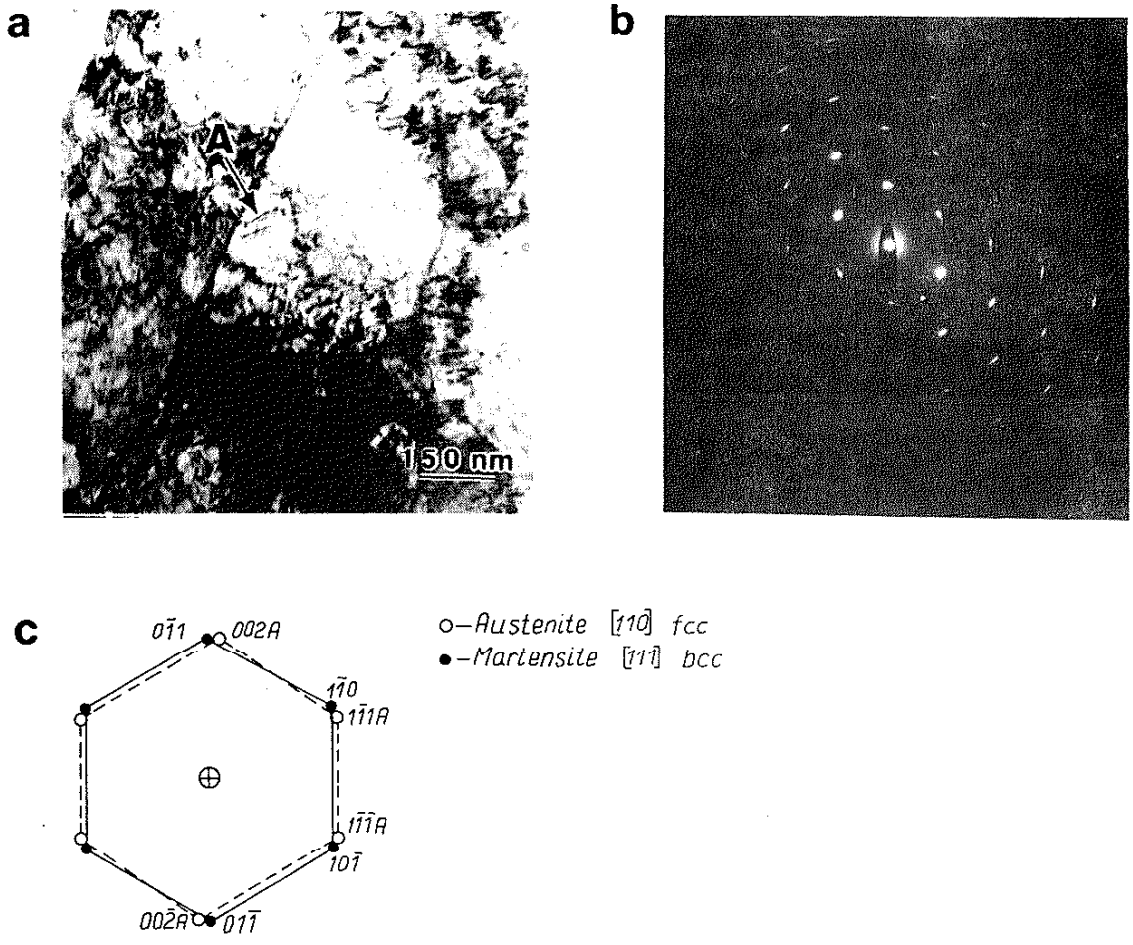

Fig. 19 Transmission electron micrographs of welded and laser dressed (LD) 18 Ni (250) maraging steel. *Aging was performed before laser-treatment*:: a) Bright-field image showing a low-carbon bcc "lath" martensite matrix and reverted austenite (indice A), b) Diffraction pattern, c) Sketch showing principal indexing.

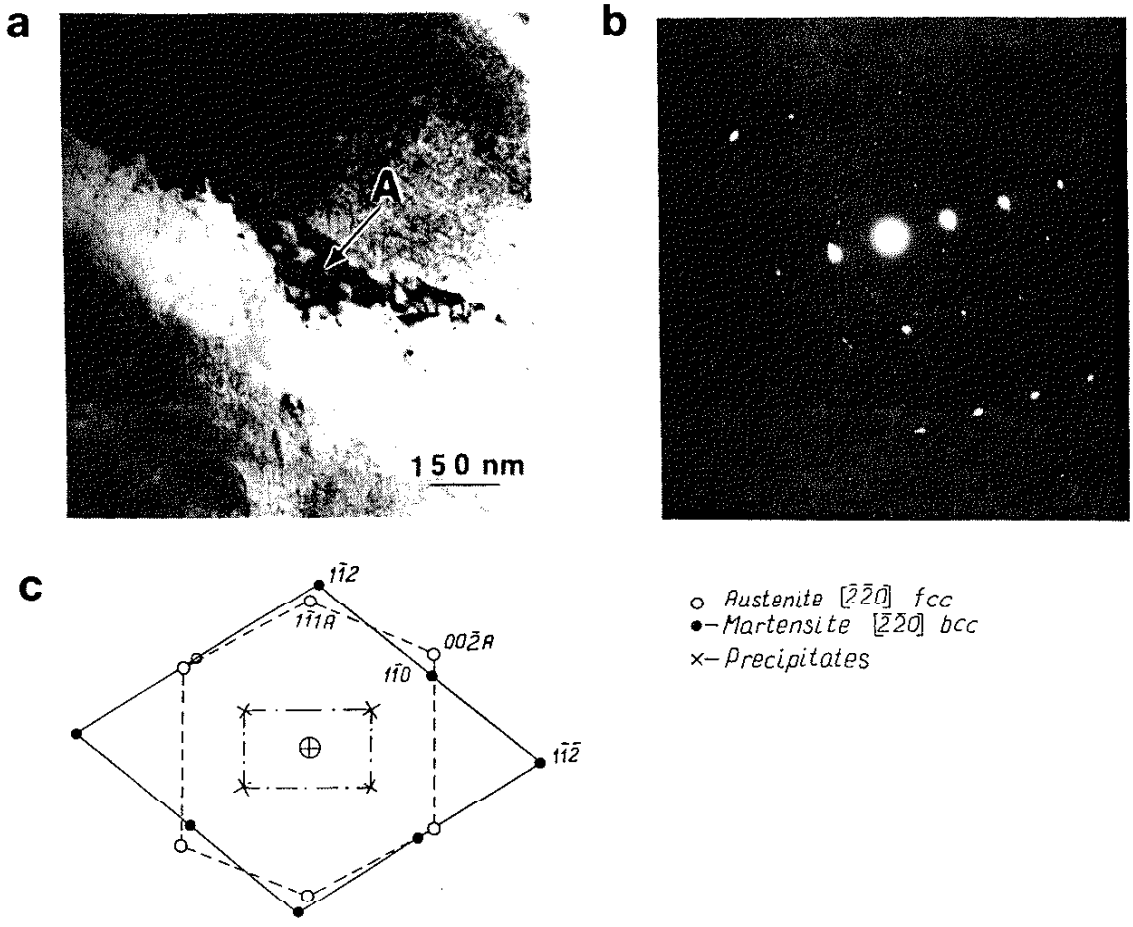

Fig. 20 Transmission electron micrographs of as-welded (AS) 18 Ni (250) maraging steel. *Aging was performed after welding*: a) Bright-field image showing a low-carbon bcc "lath" martensite matrix and reverted austenite (indice A), b) Diffraction pattern, c) Sketch showing principal indexing.

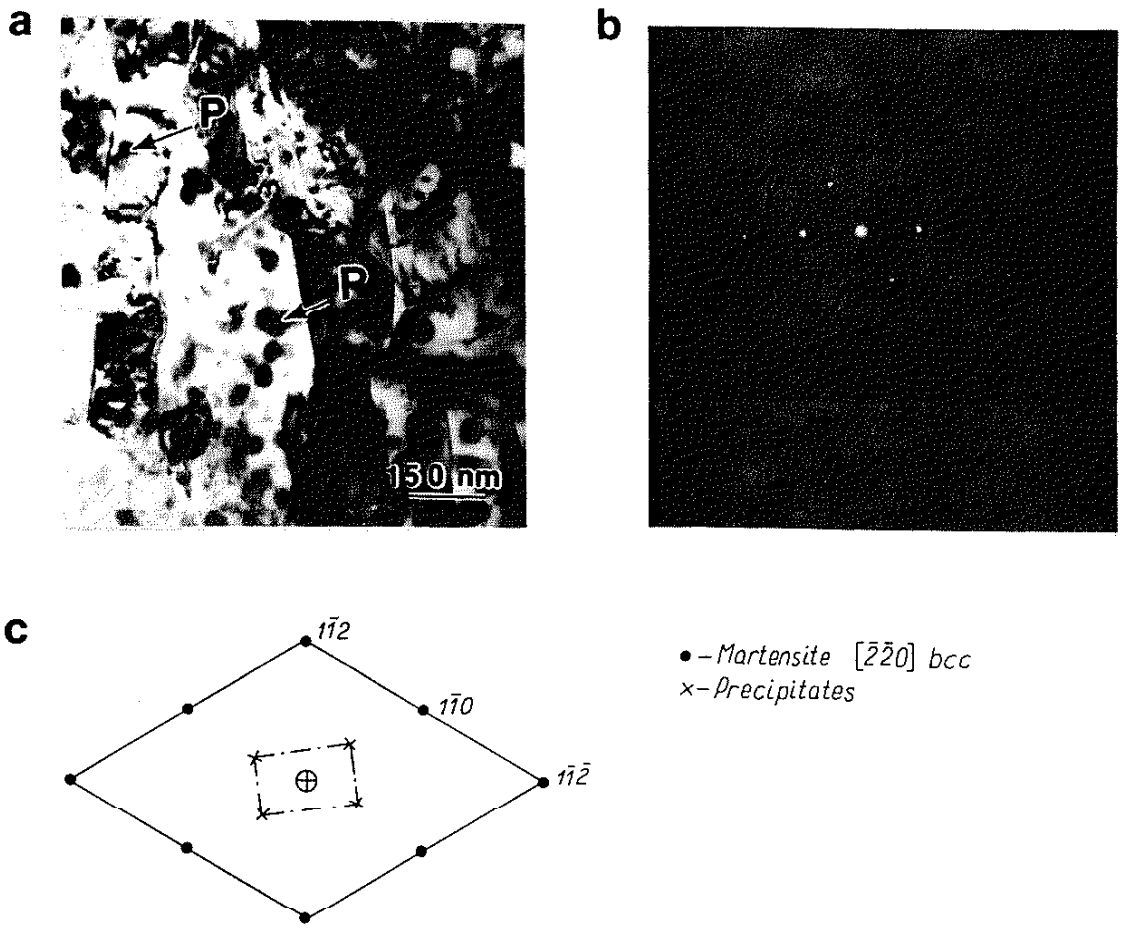

Fig. 21 Transmission electron micrographs of base metal of 18 Ni (250) maraging steel: a) Bright-field image showing a low-carbon bcc "lath" martensite matrix and precipitates (spots P), b) diffraction pattern, c) Sketch showing principal indexing.

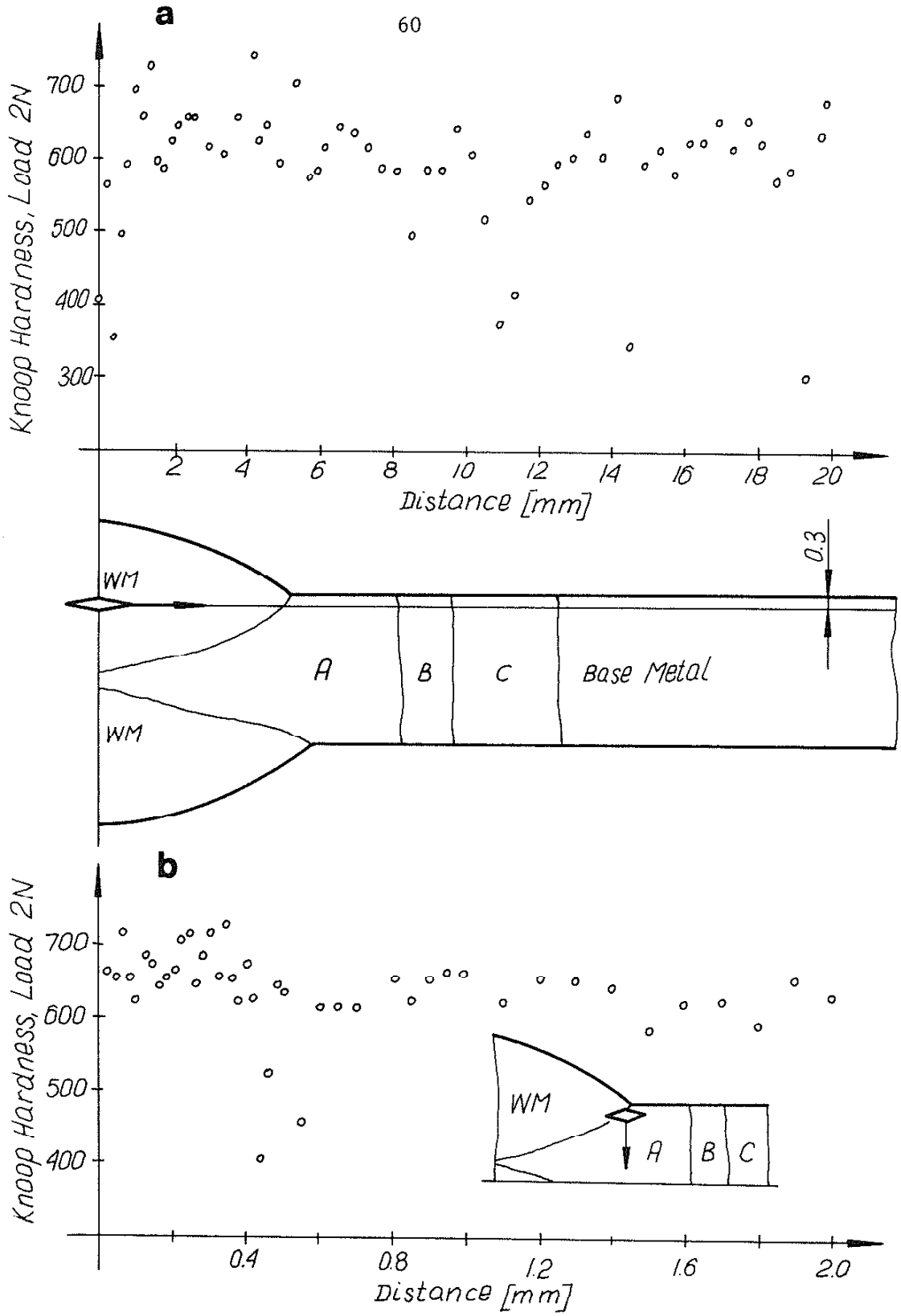

Fig. 22 Knoop hardness traverse for as-welded (AW) 18 Ni (250) maraging steel. *Aging was performed after welding*: a) At a depth of 0.3 mm below the surface along the weldment, b) Inward from the toe.

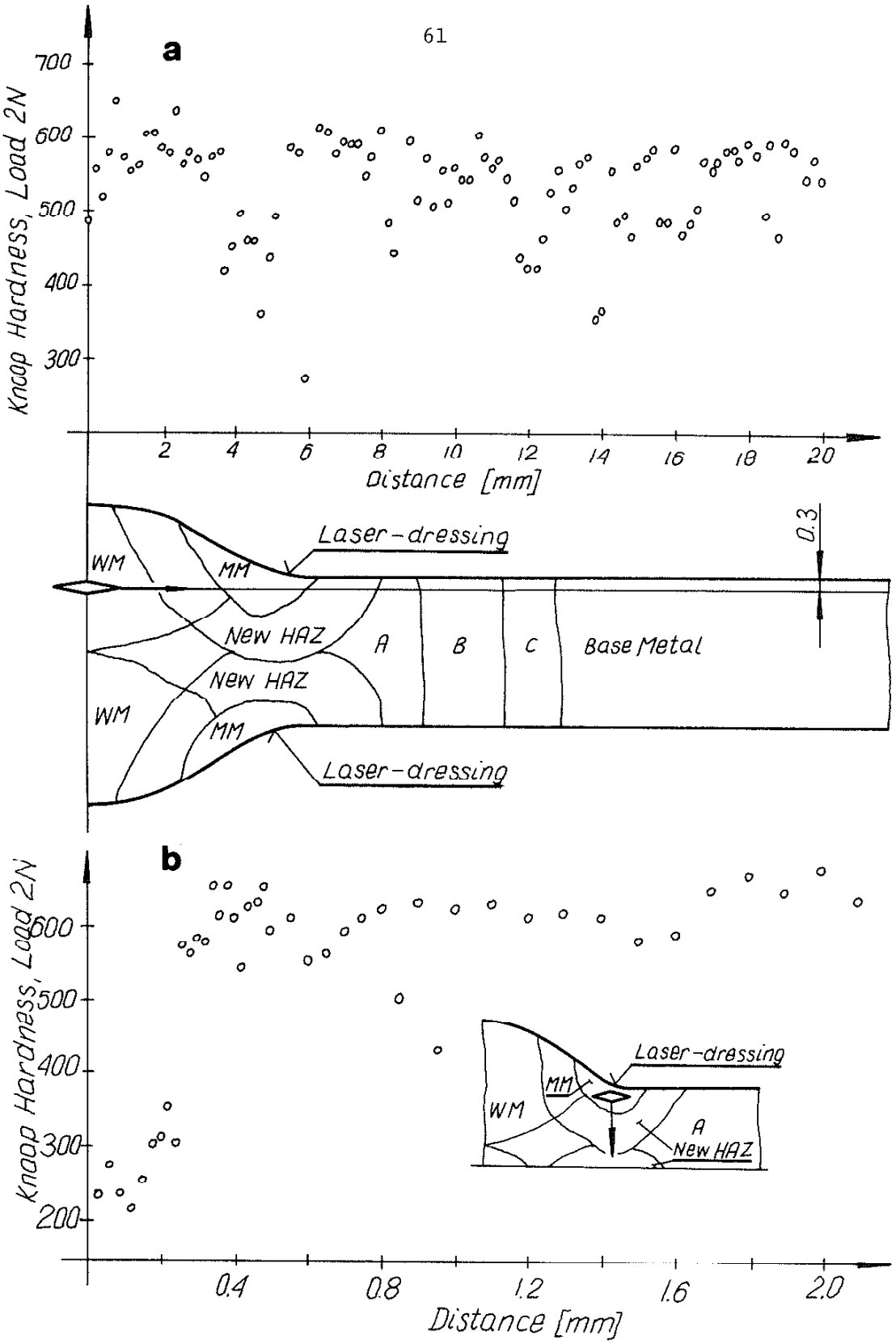

Fig. 23 Knoop hardness traverse of welded and laser dressed (LDA) 18 Ni (250) maraging steel. *Aging was performed after laser-treatment*:: a) At a depth of 0.3 mm below the surface along the weldment, b) inward from the toe.

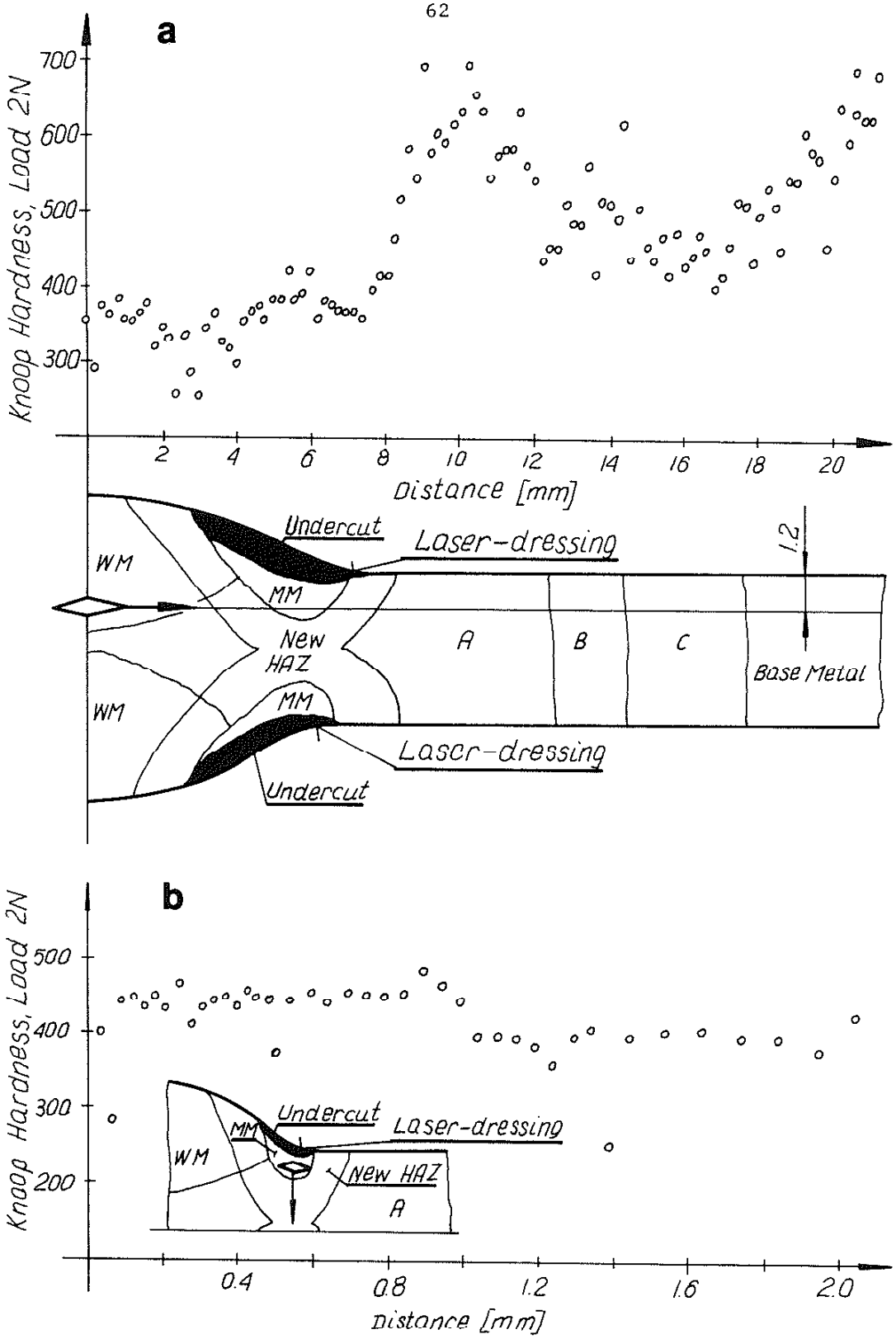

Fig. 24 Knoop hardness traverse of welded and laser-dressed (LD) 18 Ni (250) maraging steel. *Aging was performed before laser-treatment*:: a) At a depth of 1.2 mm below the surface along the weldmcnt, b) Inward from the toe.

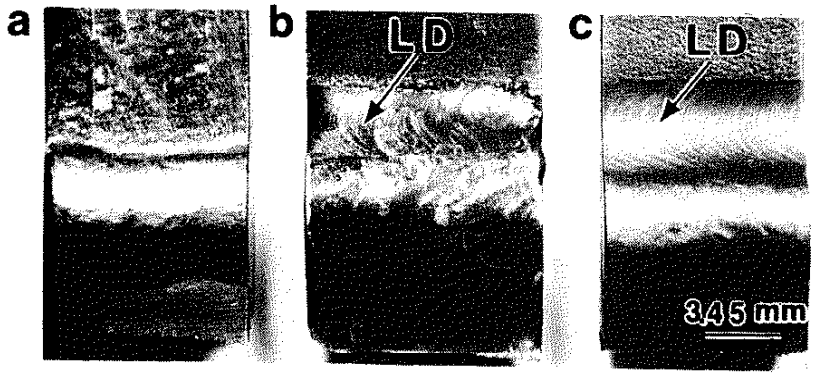

Fig. 25 Various toe configurations of welded 18 Ni (250) maraging steel: a: AW, b) LD, c) LDA.

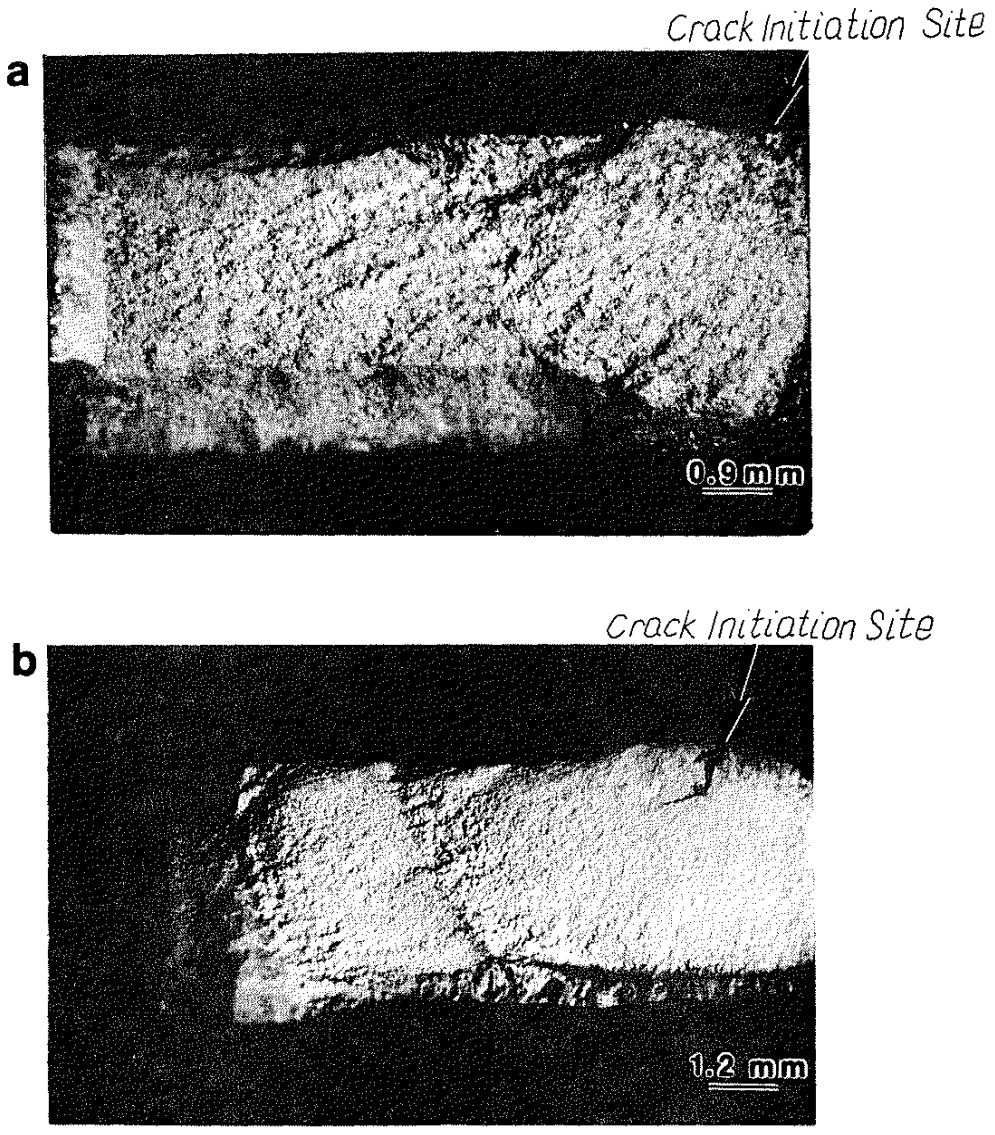

Fig. 26 Fracture surface of welded 18 Ni (250) maraging steel after fatigue test: a) As-welded (AW) -- fatigue crack initiation site was at the weld toe, b) Laser-dressed (LD) fatigue crack initiation site was at the new weld toe.

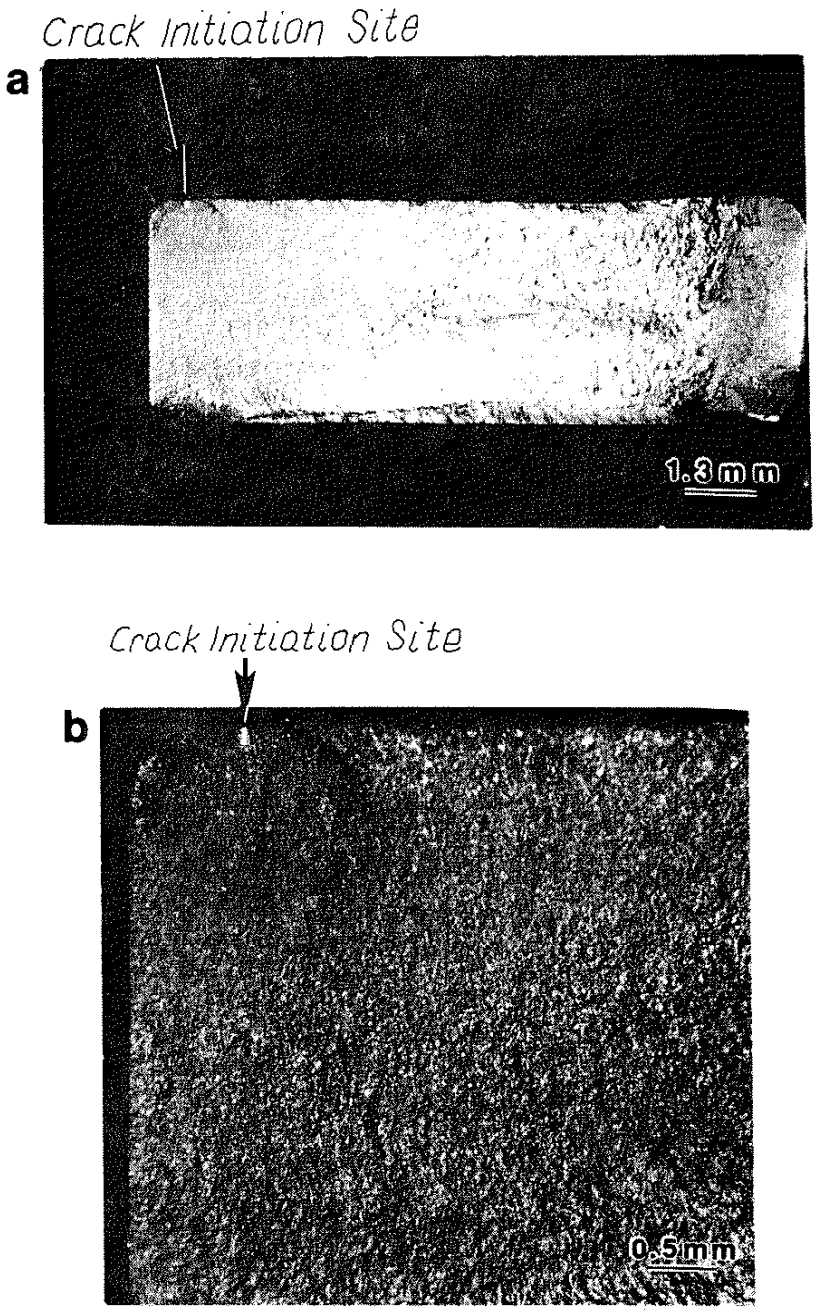

Fig. 27 Fracture surface of welded and laser-dressed (LDA) 18 Ni (250) maraging steel after fatigue test: a) fatigue crack initiation site was at the new weld toe, b) Fracture surface of a) with higher magnification.

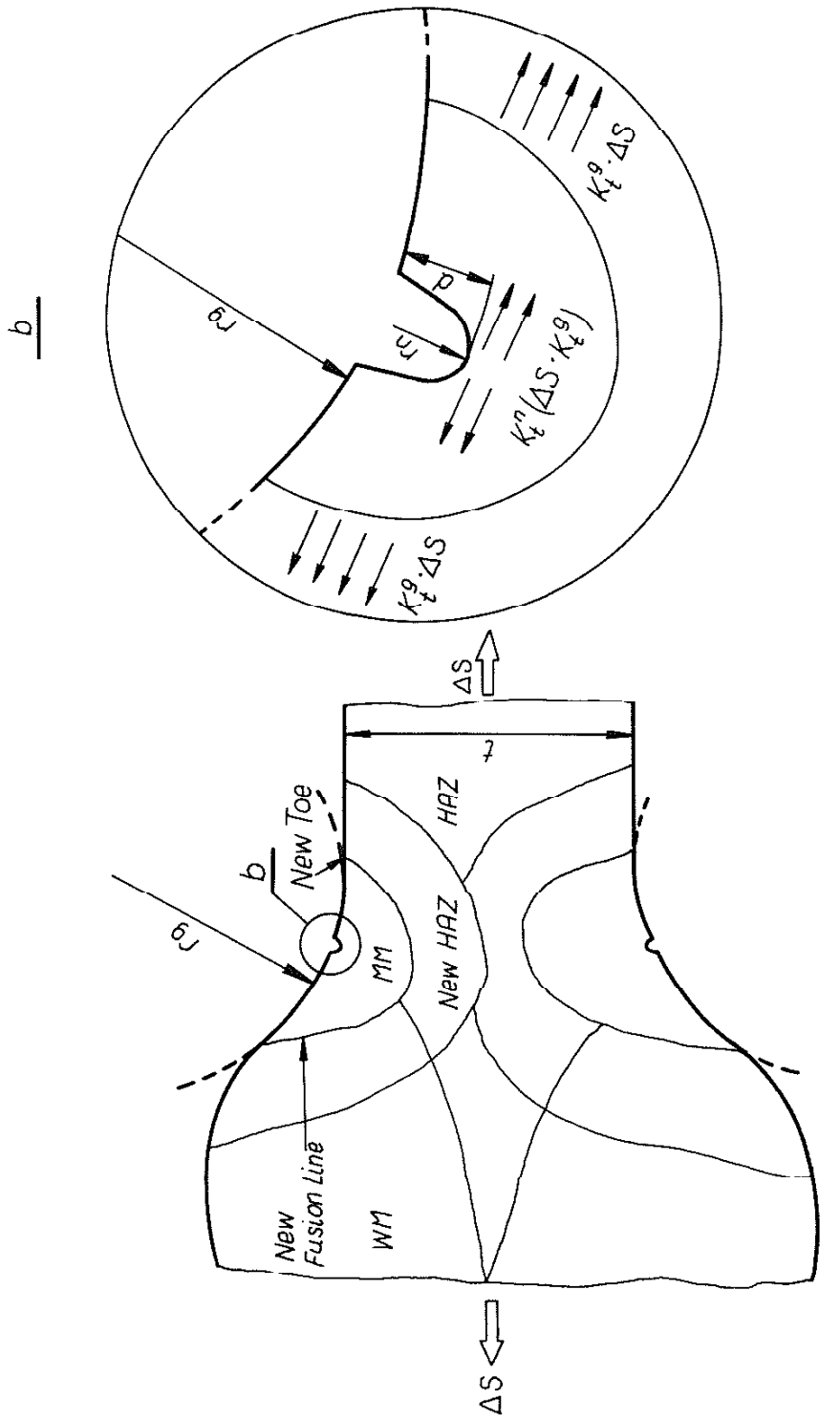

$$K_t^g = 1 + \alpha\sqrt{t/r_g} \qquad K_t^s = K_t^g \cdot K_t^n \qquad K_t^n = 1 + 2\sqrt{d/r_n}$$

Fig. 28 Schematic diagram of laser-dressed weldment [4].

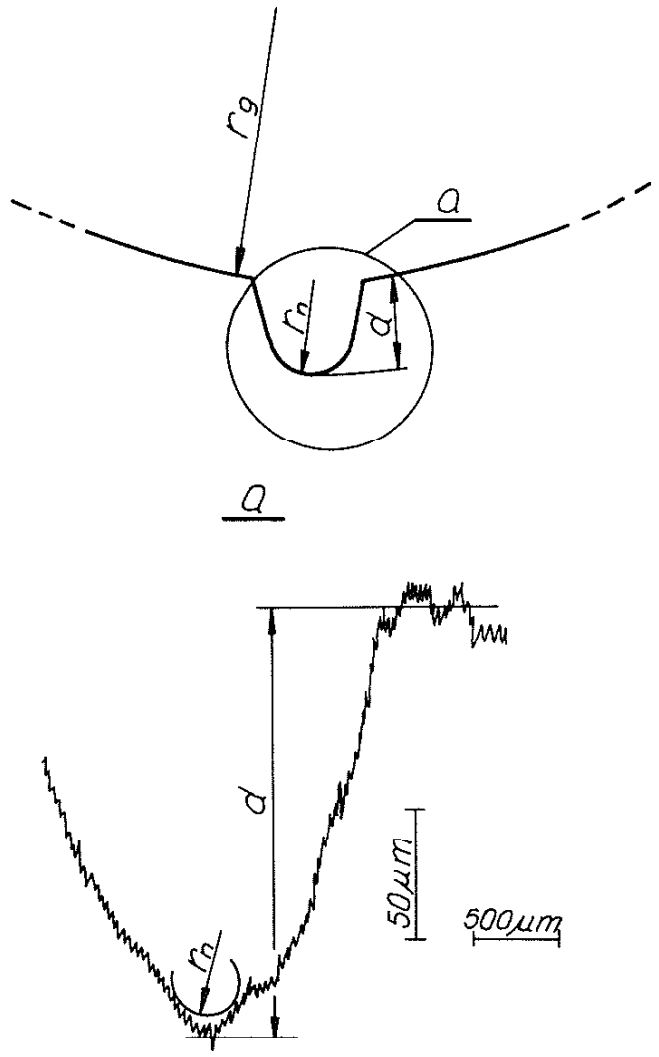

Fig. 29 Roughness profile and depth of undercut at fatigue failure sites for laser-dressed specimen.

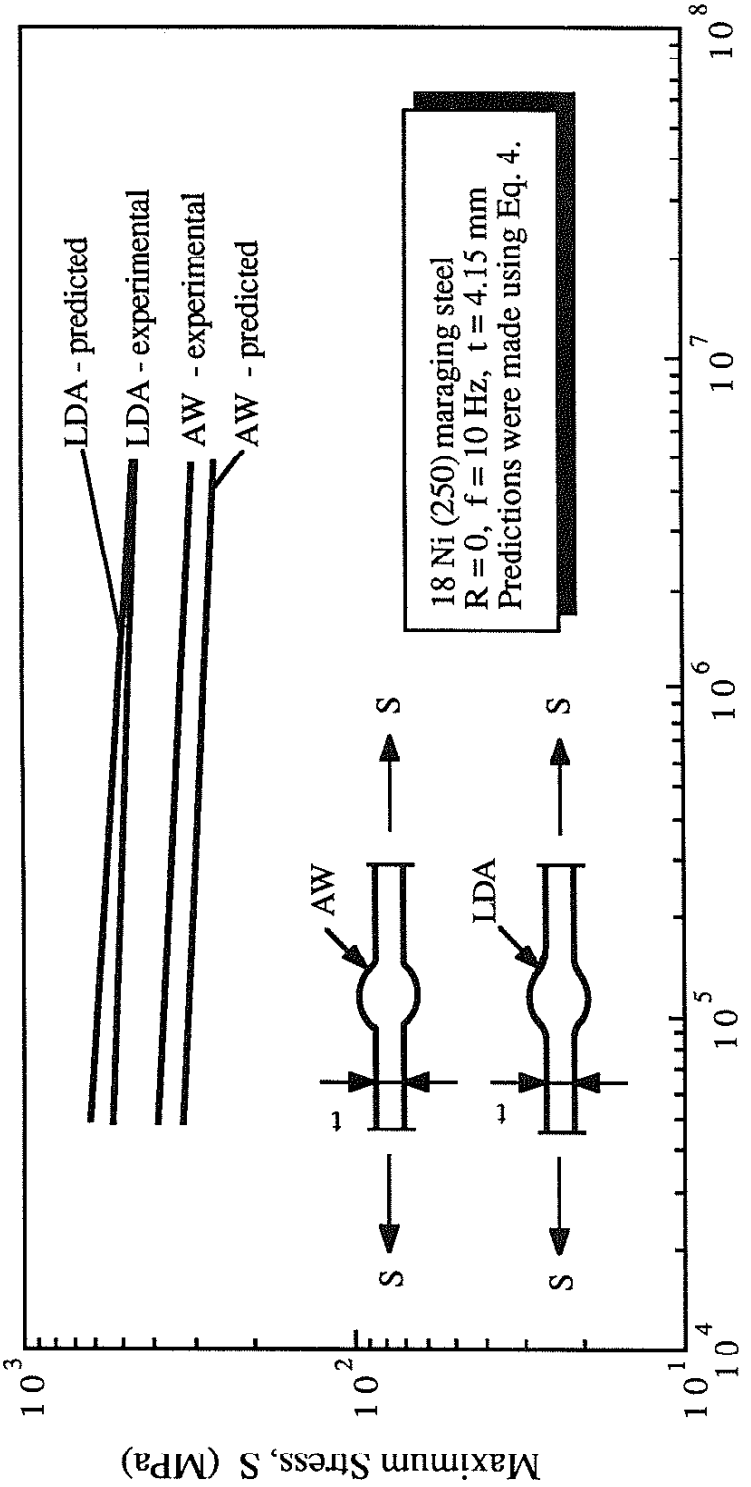

Fig. 30 Predicted and experimental fatigue results for as-welded and laser dressed specimens.